

MIDIS: MIRI uncovers *Virgil*, an extended source at $z \simeq 6.6$ with the photometric properties of Little Red Dots

EDOARDO IANI,¹ PIERLUIGI RINALDI,¹ KARINA I. CAPUTI,^{1,2} MARIANNA ANNUNZIATELLA,³ DANIAL LANGEROODI,⁴
JENS MELINDER,⁵ PABLO G. PÉREZ-GONZÁLEZ,³ JAVIER ÁLVAREZ-MÁRQUEZ,³ LEINDERT A. BOOGAARD,⁶
SARAH E. I. BOSMAN,^{6,7} LUCA COSTANTIN,³ THIBAUD MOUTARD,⁸ LUIS COLINA,³ GÖRAN ÖSTLIN,⁵
THOMAS R. GREVE,^{2,9,10} GILLIAN WRIGHT,¹¹ ALMUDENA ALONSO-HERRERO,¹² ARJAN BIK,⁵ STEVEN GILLMAN,^{2,9}
ALEJANDRO CRESPO GÓMEZ,³ JENS HJORTH,¹³ ALVARO LABIANO,^{14,12} JOHN P. PYE,¹⁵ TUOMO V. TIKKANEN,¹⁵ AND
PAUL P. VAN DER WERF¹⁶

¹*Kapteyn Astronomical Institute, University of Groningen, P.O. Box 800, 9700 AV Groningen, The Netherlands*

²*Cosmic Dawn Center (DAWN), Denmark*

³*Centro de Astrobiología (CAB), CSIC-INTA, Ctra. de Ajalvir km 4, Torrejón de Ardoz, E-28850, Madrid, Spain*

⁴*DARK, Niels Bohr Institute, University of Copenhagen, Jagtvej 155, 2200 Copenhagen, Denmark*

⁵*Department of Astronomy, Stockholm University, Oscar Klein Centre, AlbaNova University Centre, 106 91 Stockholm, Sweden*

⁶*Max Planck Institute for Astronomy, Königstuhl 17, 69117 Heidelberg, Germany*

⁷*Institute for Theoretical Physics, Heidelberg University, Philosophenweg 12, D-69120, Heidelberg, Germany*

⁸*European Space Agency (ESA), European Space Astronomy Centre (ESAC), Camino Bajo del Castillo s/n, 28692 Villanueva de la Cañada, Madrid, Spain*

⁹*DTU Space, Technical University of Denmark, Elektrovej, Building 328, 2800, Kgs. Lyngby, Denmark*

¹⁰*Department of Physics and Astronomy, University College London, Gower Street, WC1E 6BT, UK*

¹¹*UK Astronomy Technology Centre, Royal Observatory Edinburgh, Blackford Hill, Edinburgh EH9 3HJ, UK*

¹²*Centro de Astrobiología (CAB), CSIC-INTA, Camino Bajo del Castillo s/n, E-28692 Villanueva de la Cañada, Madrid, Spain*

¹³*DARK, Niels Bohr Institute, University of Copenhagen, Jagtvej 128, 2200 Copenhagen, Denmark*

¹⁴*Telespazio UK for the European Space Agency, ESAC, Camino Bajo del Castillo s/n, E-28692 Villanueva de la Cañada, Madrid, Spain*

¹⁵*School of Physics & Astronomy, Space Park Leicester, University of Leicester, 92 Corporation Road, Leicester LE4 5SP, UK*

¹⁶*Leiden Observatory, Leiden University, P.O. Box 9513, 2300 RA Leiden, The Netherlands*

ABSTRACT

We present *Virgil*, a MIRI extremely red object (MERO) detected with the F1000W filter as part of the MIRI Deep Imaging Survey (MIDIS) observations of the Hubble Ultra Deep Field (HUDF). *Virgil* is a Lyman- α emitter (LAE) at $z_{\text{spec}} = 6.6312 \pm 0.0019$ (from VLT/MUSE) with a rest-frame UV-to-optical spectral energy distribution (SED) typical of LAEs at similar redshifts. However, MIRI observations reveal an unexpected extremely red color at rest-frame near-infrared wavelengths, $F444W - F1000W = 2.33 \pm 0.06$. Such steep rise in the near-infrared, completely missed without MIRI imaging, is poorly reproduced by models including only stellar populations and hints towards the presence of an Active Galactic Nucleus (AGN). Interestingly, the overall SED shape of *Virgil* resembles that of the recently discovered population of Little Red Dots (LRDs) but does not meet their compactness criterion: at rest-frame UV-optical wavelengths *Virgil*'s morphology follows a 2D-Sérsic profile with average index $n = 0.93^{+0.85}_{-0.31}$ and $r_e = 0.43$ pkpc. Only at MIRI wavelengths *Virgil* is unresolved due to the coarser PSF. We also estimate a bolometric luminosity $L_{\text{bol}} = (8.4 - 11.1) \times 10^{44}$ erg s⁻¹ and a supermassive black hole mass $M_{\text{BH}} = (4 - 7) \times 10^7 M_{\odot}$ in agreement with recently reported values for LRDs. This discovery demonstrates the crucial importance of deep MIRI surveys to find AGN amongst high- z galaxies that otherwise would be completely missed and raises the question of how common *Virgil*-like objects could be in the early Universe.

Corresponding author: Edoardo Iani

iani@astro.rug.nl, E.Iani@rug.nl

Keywords: Galaxy formation (595) — Galaxy evolution (594) — High-redshift galaxies (734) — Stellar populations (1622) — Broad band photometry (184) — Galaxy ages (576) — JWST (2291) — Active galactic nuclei (16)

1. INTRODUCTION

Since the release of its first observations in July 2022, JWST has been revolutionizing our view on the field of the high-redshift Universe (Gardner et al. 2023). Indeed, given its remarkable sensitivity and angular resolution at infrared wavelengths, JWST is now opening up a new window on studying the early Universe, both by giving us exceptional details on known high- z sources (e.g., Bunker et al. 2023; Maiolino et al. 2023; Colina et al. 2023) and revealing the presence of new high- z galaxies (e.g., Atek et al. 2023a,b; Casey et al. 2023; Robertson et al. 2023), with some of them spectroscopically confirmed at very high redshift ($z > 10$; e.g. Curtis-Lake et al. 2023; Bunker et al. 2023; Wang et al. 2023; Castellano et al. 2024).

The Mid-Infrared Instrument (MIRI; Rieke et al. 2015; Wright et al. 2015, 2023) on JWST and, in particular, its imager (MIRIM, Bouchet et al. 2015; Dicken et al. 2024) is allowing us to study galaxies in the wavelength range from $5.6 \mu\text{m}$ through $25.5 \mu\text{m}$ at an unprecedented spatial resolution and sensitivity (Rigby et al. 2023). In its first 2 years of activity, JWST/MIRIM has demonstrated its capability to unfold the intermediate/high-redshift Universe (e.g. Iani et al. 2023; Rodighiero et al. 2023), revealing previously undetected faint galaxies (e.g. Kirkpatrick et al. 2023; Barro et al. 2023; Akins et al. 2023; Pérez-González et al. 2024a), uncovering a large population of obscured AGNs (e.g. Yang et al. 2023), and characterising the physical properties of distant galaxies in great detail (e.g. Colina et al. 2023; Álvarez-Márquez et al. 2023a), including their morphologies (e.g. Boogaard et al. 2023, Gillman et al. *in prep.*). MIRI also has a unique role in the study of early galaxies. By leveraging the deepest image of the Universe at $5.6 \mu\text{m}$ (Östlin et al. *in prep.*), Rinaldi et al. (2023a,b) detected for the first time the $\text{H}\alpha$ emission line in individual galaxies at $z \approx 7 - 9$.

Before JWST, studying high-redshift objects was challenging. Notably, the key to discovering these sources was a large (red) color between a near-infrared and an optical band. The first discoveries of these “Extremely Red Objects” (EROs) were made by using ground-based near-infrared telescopes which enabled the detection of a large variety of galaxies, from high-redshift quasars to very young and dust-rich objects (e.g., Elston et al. 1988; Graham & Dey 1996; Caputi et al. 2004). With the advent of *Spitzer* and its Infrared Array Camera (IRAC;

Fazio et al. 2004), the search for EROs was pushed to even longer wavelengths. In this regard, several studies reported the presence of galaxies that were bright in IRAC, but extremely faint or even invisible in deep optical images (“HST-dark” galaxies, e.g. Yan et al. 2004; Caputi et al. 2012; Franco et al. 2018; Wang et al. 2019; Alcalde Pampliega et al. 2019).

Some EROs have been linked to the discovery of submillimeter galaxies (SMG; e.g., Hughes et al. 1998). Indeed, many EROs are identified as dusty galaxies that are visible in mid- and far-infrared surveys under various classifications and names, beginning with SMGs (e.g., Blain et al. 2002; Chapman et al. 2005), as well as (hot) dust-obscured galaxies (DOGs/hotDOGs; e.g., Dey et al. 2008; Narayanan et al. 2010; Tsai et al. 2015), extremely red quasars (ERQs; e.g., Hamann et al. 2017), or, from a more observational point of view, (ultra-)luminous infrared galaxies (U/LIRGs; e.g. Sanders & Mirabel 1996; Elbaz et al. 2002; Pérez-González et al. 2005; Le Floch et al. 2005; Caputi et al. 2007; Magnelli et al. 2009; Madau & Dickinson 2014). EROs selected at fainter magnitudes and longer wavelengths include galaxies identified using the Lyman break technique (Steidel et al. 1996), extending the colour selection to increasingly higher redshifts (e.g., Bouwens et al. 2011).

Crucially, JWST has now the capability to push forward the identification and characterization of EROs (e.g. Chen et al. 2022; Cheng et al. 2023; Price et al. 2023; Gillman et al. 2023; Crespo et al. 2024). Some new galaxy populations are being discovered, such as high redshift galaxies with very high equivalent width emission lines (Rinaldi et al. 2023a; Boyett et al. 2024; van Mierlo et al. 2023; Álvarez-Márquez et al. 2023b) and the so-called “Little Red Dots” (LRDs; Labbe et al. 2023; Matthee et al. 2024; Barro et al. 2023; Kokorev et al. 2024; Langeroodi & Hjorth 2023a; Pérez-González et al. 2024a), a class of red compact sources with distinct spectral energy distributions showing clear Lyman and Balmer breaks and a characteristic “v-shaped” SED (in the $\lambda - f_\lambda$ plane). For LRDs, such red colors at rest-frame near-infrared wavelengths would be due to the presence of an AGN, as also supported by spectroscopic findings of broad components in their Balmer lines (e.g. $\text{H}\alpha$, $\text{H}\beta$) suggesting active accretion onto supermassive black holes (SMBH; Furtak et al. 2023a; Fujimoto et al. 2023; Greene et al. 2024; Killi et al. 2023; Kocevski et al.

2023; Kokorev et al. 2023; Übler et al. 2023; Matthee et al. 2024).

Even more exciting is the capability of the MIRI deep surveys to discover exotic objects that remain undetected by even the deepest NIRC*am* surveys available on the market, such as the JWST Advanced Deep Extragalactic Survey (JADES; Eisenstein et al. 2023a; Rieke & the JADES Collaboration 2023). In this regard, the *Cerberus* object (Pérez-González et al. 2024b) represents the first MIRI Extremely Red Object (MERO) discovered in the era of JWST.

In this paper, we present and study *Virgil*, a MERO found in the MIRI Deep Imaging Survey (MIDIS, Östlin et al. *in prep.*) F1000W imaging ($\alpha(\text{J2000.0}) = 03:32:37.9370$ (hours); $\delta(\text{J2000.0}) = -27:47:10.712$ (degrees)). The source is clearly detected in the NIRC*am* bands and it has been already catalogued in both JADES DR2 and VLT/MUSE catalogues (Bacon et al. 2023a; Rieke & the JADES Collaboration 2023). The latter reveals that this source is a Lyman- α emitter (LAE) at $z_{\text{spec}} = 6.6312 \pm 0.0019$. *Virgil* shows an extremely red color between 4.4 and 10 μm and is also red with respect to the bluest MIRI band (F560W), as revealed by MIDIS F560W imaging.

This paper is organized as follows. In §2 we briefly describe the datasets used and in particular the MIDIS 10 μm MIRI imaging and the ancillary HST and JWST NIRC*am* and MIRI observations. In §3 we describe the identification of *Virgil*, the assessment of its redshift, the decontamination of its light from the nearby LAE at $z \simeq 4.77$, the analysis of its morphology, and the extraction of its multi-wavelength photometry. In §4 we discuss the possible nature and the importance of MIRI imaging for the detection and characterisation of such an object. Finally, we summarise our findings and present our conclusions in §5.

Throughout the paper, we assume a flat cosmology with $\Omega_M = 0.3$, $\Omega_\Lambda = 0.7$, and a Hubble constant $H_0 = 70 \text{ km s}^{-1} \text{ Mpc}^{-1}$. We adopt the AB magnitudes (Oke & Gunn 1983). All stellar mass and SFR estimations assume a universal Chabrier initial mass function (IMF; Chabrier 2003). Finally, unless differently stated, we report the average 5σ depth for point-like sources of the available NIRC*am* and MIRI imaging of the MIDIS area as measured in circular apertures of $r = 0''.2$ (NIRC*am*) and $r = 0''.3$ (MIRI) as outlined by Östlin et al. (*in prep.*) and taking into account effects of pixel correlation as explained in Fruchter & Hook (2002). The depth estimates are not corrected for aperture.

2. DATASETS

2.1. MIRI F1000W data

MIRI data in the F1000W filter were taken as part of *The MIRI Deep Imaging Survey* (MIDIS, PID: 1283; PI: G. Östlin; Östlin et al., *in prep.*) in December 2023. The observation consisted of 11 exposures, each with 100 groups and 7 integrations, for a total on-source exposure time of 30.8 ks, centered on the Hubble Ultra Deep Field (HUDF, Beckwith et al. 2006). The dithering pattern was set to large-size cycling, with the 11 exposures taken in different positions on the sky separated by up to $10''$. This dithering pattern, with no repeated positions, is crucial for the detection of faint sources, such as the one presented here, and their distinction from detector artifacts.

The reduction of the MIRI data is described in Pérez-González et al. (2024b). Briefly, a super-background strategy is used to build background maps for every single image using all the other exposures (since they were taken during the same campaign), which results in a very homogeneous background (in terms of level and noise). Known sources are masked to avoid biasing the determination of the very local background in the super-background frame. Our F1000W image, reduced with 60 milliarcsec pixels, presents an average 5σ depth of 26.4 mag. We present the MIDIS F1000W data in Figure 1 (top panels) with an RGB image built in combination with the NIRC*am* long-wavelength channels F277W and F356W.

2.2. Ancillary data

We complement our MIRI observations at 10 μm with a rich set of photometric and spectroscopic data publicly available. In particular, we extend our dataset including more MIRI observations, HST and JWST/NIRC*am* filters, the Atacama Large Millimeter/submillimeter Array (ALMA) surveys and deep optical integral field spectroscopy by the Multi Unit Spectroscopic Explorer (MUSE) at the Very Large Telescope (VLT). We briefly summarise these ancillary datasets in the following sections.

2.2.1. Additional MIRI data

We combine the recently acquired MIDIS F1000W data with the F560W ultra-deep observations also carried out by MIDIS in December 2022 and January 2023. A thorough description of this dataset is presented in Östlin et al. (*in prep.*). These observations consist of ~ 41 hours on source taken in the HUDF, reaching a 5σ depth of 28.6 mag. We add to the MIDIS observations the publicly available MIRI data gathered by the *Systematic Mid-infrared Instrument Legacy Extragalactic Survey* (SMILES, PID 1207; PI: G. Rieke; Lyu et al. 2023) in the F770W, F1280W, F1500W, F1800W, F2100W and F2550W bands. We reduce the SMILES

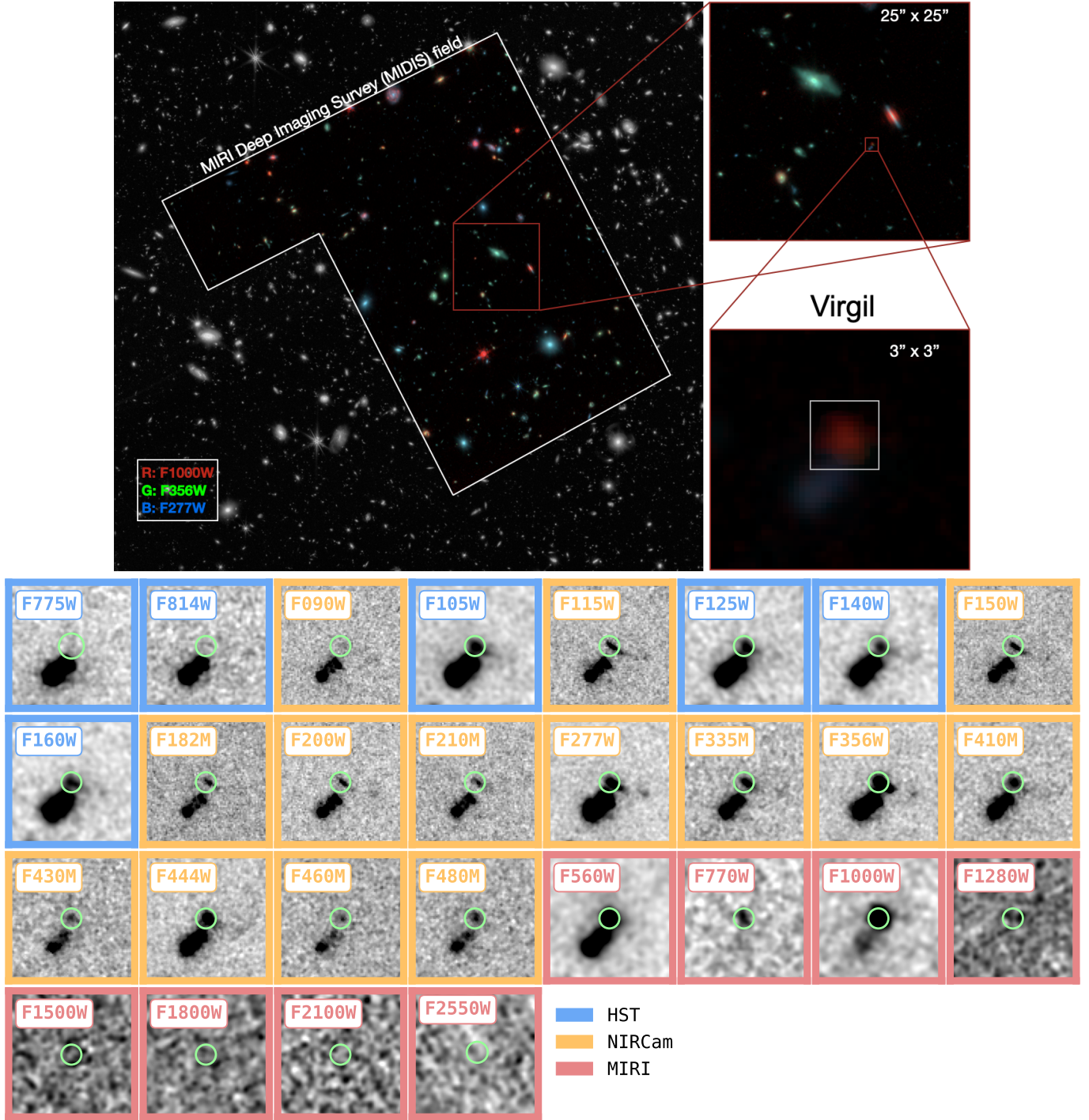


Figure 1. Top Panel: RGB composition of the MIDIS field. The color images have been built with JADES data in 2 NIRCam filters, F277W and F356W, and the MIDIS MIRI F1000W filter (all convolved to the same PSF as MIRI/F1000W). In the background, we show the HUDF JADES data in gray scale. We show a series of zoomed-in RGB frames that lead to the MIRI Extremely Red Object source, *Virgil* ($\alpha(\text{J2000.0}) = 03:32:37.9370$ (hours); $\delta(\text{J2000.0}) = -27:47:10.712$ (degrees)). The *Virgil* object is highlighted with a square in the RGB frame at the bottom right. **Bottom Panel:** Cutouts ($2''.5 \times 2''.5$) of *Virgil* from HST/ACS and WFC3 (F775W, F814W, F105W, F125W, F140W, and F160W), JWST/NIRCam (F090W, F115W, F150W, F200W, F210M, F277W, F335M, F356W, F410M, F430M, F444W, F460M, and F480M) and JWST/MIRI (F560W, F770W, F1000W, F1280W, F1500W, F1800W, F2100W, and F2550W). We highlight *Virgil* with a green circle ($r = 0''.2$). HST cutouts below $0.7 \mu\text{m}$ are not shown here.

images following the same methodology applied to the MIDIS dataset and obtain images with a 5σ depth of about 26.2 (F770W), 25.0 (F1280W), 24.9 (F1500W), 24.1 (F1800W), 23.6 (F2100W) and 21.8 (F2550W) mag, respectively.

2.2.2. NIRCam data

We complement the MIRI data with NIRCam imaging taken by *The JWST Advanced Deep Extragalactic Survey* (JADES, PIDs: 1180, 1210; P.I.: D. Eisenstein, N. Luetzgendorf; Eisenstein et al. 2023b), Data Release 2 (Eisenstein et al. 2023c), which includes also observations from the *JWST Extragalactic Medium-band Survey* (JEMS, PID: 1963; PIs: C. C. Williams, S. Tacchella, M. Maseda; Williams et al. 2023) and *The First Reionization Epoch Spectroscopically Complete Observations* (FRESCO, (FRESCO, PID: 1895; PI: P. Oesch; Oesch et al. 2023a). This dataset provides a total of 14 bands from 0.9 to 4.8 μm (F090W, F115W, F150W, F182M, F200W, F210M, F277W, F335M, F356W, F410M, F430M, F444W, F460M, F480M) with 5σ depths ranging from 30.5 to 30.9 mag.

2.2.3. HST data

We obtain all the HST images over the HUDF from the Hubble Legacy Field GOODS-S (HLF-GOODS-S Whitaker et al. 2019). The HLF-GOODS-S provides 13 HST bands covering a wide range of wavelengths (0.2–1.6 μm), from the UV (WFC3/UVIS F225W, F275W, and F336W filters), optical (ACS/WFC F435W, F606W, F775W, F814W, and F850LP filters), to near-infrared (WFC3/IR F098M, F105W, F125W, F140W and F160W filters). In this paper, we only made use of the deepest ones (i.e., F435W, F606W, F775W, F814W, F850LP, F105W, F125W, F140W, F160W). We refer the reader to Whitaker et al. (2019) for more detailed information on these observations.¹

2.2.4. MUSE data

The HUDF has been extensively studied with MUSE (Bacon et al. 2010) at VLT as part of the MOSAIC and UDF-10 fields (GTO programs 094.A-0289(B), 095.A-0010(A), 096.A-0045(A) and 096.A-0045(B), PI: R. Bacon) and the most recent MXDF observations (GTO Large Program 1101.A-0127, PI: R. Bacon). These observations cover a spectral wavelength range between 4750 - 9350 \AA with a spectral resolving power (R) that varies from 1770 (4800 \AA) to 3590 (9300 \AA) and have a PSF (at 7750 \AA), that can be described by a Moffat

function (Moffat 1969) that varies from FWHM = 0''.45 and $\beta = 1.89$ (MXDF), to FWHM = 0''.60 and $\beta = 2.80$ (UDF-10), and to FWHM = 0''.63 and $\beta = 2.80$ (MOSAIC), see Bacon et al. (2023a) and their Table 4. In the MIDIS area, these observations have exceeded total exposure times of 140 hours, although the distribution of the depth in flux is not uniform across the whole area. More details about the HUDF MUSE surveys can be found in Bacon et al. (2017, 2023b). In our study we use the fully reduced MUSE datacubes for the MOSAIC + UDF-10 and MXDF programs, as well as the catalog of detected sources and corresponding redshifts presented in Bacon et al. (2023a).²

2.2.5. ALMA data

The Atacama Large Millimeter/submillimeter Array (ALMA) Spectroscopic Survey in the Hubble Ultra Deep Field (ASPECS) is a Cycle 4 Large Program over a 4.6 arcmin² scan at 1.2 mm (band 6; Decarli et al. 2020; González-López et al. 2020) and 3.0 mm (band 3; Decarli et al. 2019; González-López et al. 2019). The ultra-deep 1.2 mm data reaches an rms sensitivity of 9.3 $\mu\text{Jy}/\text{beam}$, with beam dimensions of 1''.5 \times 1''.1. The 3.0 mm data reaches 1.4 $\mu\text{Jy}/\text{beam}$, with a 1''.8 \times 1''.5 beam. We download the fully reduced ALMA images from the official ASPECS website.³

3. SELECTION AND PROPERTIES OF THE MIRI EXTREMELY RED OBJECT VIRGIL

In this paper, we present *Virgil* ($\alpha(\text{J2000.0}) = 03:32:37.9370$ (hours); $\delta(\text{J2000.0}) = -27:47:10.712$ (degrees)), a source in the deep MIDIS F1000W image of the HUDF, which is counterpart to a LAE at $z = 6.6312$ from MUSE/VLT (§3.2). Despite being already known from shorter wavelength data (Bacon et al. 2023a; Rieke et al. 2023; Eisenstein et al. 2023c), new important insights on the nature of this object come from the new deep MIRI observations at 10 μm . In particular, *Virgil* displays an extreme F444W – F1000W red color (≥ 2) that classifies it as an ERO. Since the ERO nature of this source can only be determined with MIRI, we refer to it as MERO.

3.1. Identification of the MERO Virgil

In order to select MEROs, we make use of the SEXTRACTOR software (Bertin & Arnouts 1996a) directly using the MIRI/F1000W map as detection image. We

¹ The HLF-GOODS-S imaging is available at <https://archive.stsci.edu/prepds/hlf/>;

² The MUSE cubes can be obtained at <https://amused.univ-lyon1.fr/project/UDF/HUDF/>;

³ The ASPECS images are available at <https://almascience.org/alma-data/lp/ASPECS/>;

follow the hot-mode extraction described in Galametz et al. (2013), which is particularly effective for detecting extremely faint sources and construct a photometric MIRI/F1000W catalog based on the SEXTRACTOR magnitude estimates `MAG_AUTO`. We cross-match our catalog (using a $0''.2$ search radius) to the official JADES DR2 catalog published by Eisenstein et al. (2023c) to only consider those sources showing a red F444W - F1000W color ($F444W - F1000W \geq 1.5$) and a robust F1000W detection ($S/N \geq 5$). After the recently reported MERO *Cerberus* found in the MIDIS field ($F444W - F1000W > 3.5$ mag; Pérez-González et al. 2024b), *Virgil* is the second reddest object we find in our sample, having $F444W - F1000W = 2.33 \pm 0.06$. We name this MERO *Virgil*, to acknowledge the fact that it is very close in projection to *Cerberus* (separation $\delta \approx 2''.3$). An RGB image of the source built with NIRCcam and MIRI data is presented in Figure 1, jointly with a series of postage stamps that show *Virgil* from 0.7 to $21\mu\text{m}$.

3.2. Redshift assessment of *Virgil*

In the JADES DR2 catalogue (Eisenstein et al. 2023a), *Virgil* is listed with ID 206038 and a photometric redshift $z_{\text{phot}} \approx 6.62$. This redshift estimate agrees with the fact that our source appears to be a NIRCcam F090W drop out, see the cutouts presented in Figure 1.

However, to better constrain the properties of our target, we investigate if we can derive a spectroscopic redshift z_{spec} from the available MUSE observations. In fact, based on the z_{phot} reported by the JADES DR2 catalog, the MUSE data should cover *Virgil*'s rest-frame UV emission. Therefore, we look for the possible presence of emission lines, and in particular, of the Ly α line in the MUSE cube. To do so, we extract the MUSE 1D spectrum at the coordinates of our target within circular apertures of different sizes ($r = 0''.4, 0''.8$). Despite being strongly contaminated by the extended rest-frame UV emission of a close-by LAE at $z_{\text{spec}} \simeq 4.77$ (ID 53; Bacon et al. 2023a), in the MUSE 1D spectrum we find a spectral feature appearing only at the position of the MIRI extremely red object. This line cannot be explained by any known emission line in the UV spectrum of galaxies at $z = 4.77$ and falls at the expected wavelength of the Ly α at $z \simeq 6.63$ (i.e. $\approx 9280 \text{ \AA}$, see right panel of Figure 2). The classification of this spectral line as *Virgil*'s Ly α is in agreement with the publicly available catalogue of MUSE-detected sources by Bacon et al. (2023a). Particularly, Bacon et al. (2023a) list this source (ID 7699) as an LAE at a spectroscopic redshift $z_{\text{spec}} = 6.6312 \pm 0.0019$

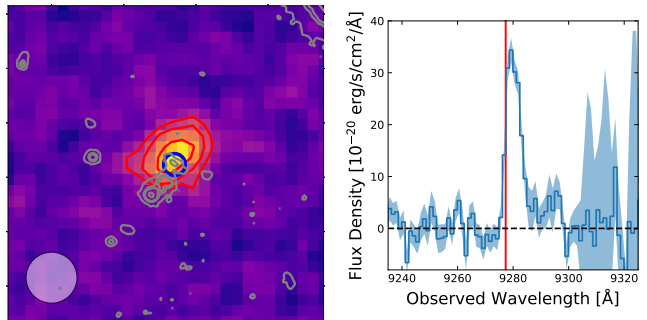


Figure 2. **Left panel:** MUSE pseudo-narrow-band image ($6'' \times 6''$) of *Virgil*'s Ly α emission. Red contours are drawn at 2, 3 and 5 σ while gray contours are representative of the JWST/NIRCcam F200W imaging. The source position is indicated with $0.2''$ radius circle. The MUSE PSF is shown in the bottom left corner. **Right panel:** MUSE 1D spectrum of *Virgil*'s Ly α . The vertical red line is indicative of the expected position of the Ly α at $z = 6.6312$.

(`quality_flag` = 2, i.e. good confidence⁴) with a Ly α flux $F(\text{Ly}\alpha) \approx 1.6 \times 10^{-18} \text{ erg s}^{-1} \text{ cm}^{-2}$ (corresponding to a Ly α luminosity $L(\text{Ly}\alpha) \approx 8.1 \times 10^{41} \text{ erg s}^{-1}$) and $S/N \approx 8$. Therefore, we assume $z_{\text{spec}} = 6.6312 \pm 0.0019$ as *Virgil*'s redshift for the rest of our analysis. Nonetheless, given the wealth of recent spectroscopic campaigns in the HUDF, we also verify if our target had been observed by the FRESCO (PID: 1895; PI: P. Oesch, Oesch et al. 2023b), the NGDEEP (PID: 2079; PI: Finkelstein, Bagley et al. 2024) and JADES surveys. Unfortunately, our target is not detected in FRESCO's NIRCcam Wide Field Slitless Spectroscopy (WFSS) observations⁵, nor in the NGDEEP's NIRISS WFSS observations⁶. Finally, the NIRSpc Micro Shutter Array (MSA) observations from JADES (D'Eugenio et al. 2024) in HUDF did not cover the area of our target.

3.3. Removal of *Virgil*'s contaminant

In the JADES DR2 catalog, *Virgil*'s contaminant at $z \approx 4.77$ (Bacon et al. 2023a; see also Matthee et al. 2022) turns out to be constituted by two sources: ID 285736 and ID 206035. With respect to *Virgil*'s location, ID 285736 is about $0''.4$ away while ID 206035 has a separation of $0''.7$ both in the south-east direc-

⁴ An LAE with `quality_flag` = 2 has a Ly α $S/N > 5$ and a width and asymmetry compatible with typical Ly α line shapes (Bacon et al. 2023a);

⁵ The FRESCO line sensitivity (estimated for compact sources and integrated over the full extent of the line) is $\approx 2 \times 10^{-18} \text{ erg s}^{-1} \text{ cm}^{-2}$ at 5σ (Oesch et al. 2023b);

⁶ The NGDEEP spectroscopy was carried out in the F115W, F150W and F200W filters reaching 5σ integrated emission line limits of $1.2, 1.3$ and $1.5 \times 10^{-18} \text{ erg s}^{-1} \text{ cm}^{-2}$, respectively (Bagley et al. 2024);

tion. To avoid the contamination of *Virgil*'s photometry due to this extended lower redshift LAE, we model and subtract its contribution at all wavelengths. To do so, we resort to the galaxy morphology modeling tool ASTROPHOT (Stone et al. 2023). With ASTROPHOT, we model ID 285736 and ID 206035 with single Sérsic profiles while masking *Virgil*. From the first results, we find that to improve the quality of the residuals in several filters, it is necessary to introduce an optional third Sérsic component between ID 285736 and ID 206035, see also Matthee et al. (2022). In Figure 3, we present the residuals of the best-fit models obtained with ASTROPHOT for some of the available filters.

3.4. *Virgil*'s morphology

After the removal of *Virgil*'s contaminant and before extracting its photometry (see §3.3), we briefly investigate *Virgil*'s morphology.

At NIRCcam wavelengths our target is clearly elongated in the south-west direction and features a tail that seems to end up in a (faint) clump (*Beatrix*; $\alpha(\text{J2000.0}) = 03:32:37.8844$ (hours); $\delta(\text{J2000.0}) = -27:47:10.979$) that can be detected at several NIRCcam wavelengths but is completely missing in the MIRI imaging, see Figure 3. On the basis of the current data, it is difficult to assess whether *Beatrix* is a clump of *Virgil* or a different object at a different redshift (see §3.5). However, if confirmed at *Virgil*'s redshift, the separation between *Virgil* and *Beatrix* ($\delta \approx 0''.75$) would correspond to a projected distance of about 4 pkpc and, considering its point-like nature, a size $r \lesssim 0''.06 \simeq 0.3$ pkpc.

At MIRI wavelengths, *Virgil* is unresolved due to the coarser MIRI PSF. This is confirmed by the extraction of *Virgil*'s radial surface brightness profile and its comparison with the PSF trend in the different NIRCcam and MIRI filters. After masking *Beatrix* and other close-by sources, the extracted surface brightness profile shows that *Virgil* is an extended object at most wavelengths, while at 7.7 and 10 μm , the MIRI PSF dominates its morphology. If we fit a Sérsic profile (Sérsic 1963) to the SB radial profiles of the different NIRCcam filters, we find a median value of the Sérsic index $n = 0.93_{-0.31}^{+0.85}$ (16th and 84th percentiles) and an effective radius $r_e \simeq 0.08'' = 0.43$ pkpc. Both parameters are in agreement with the expected values of galaxy sizes and Sérsic indices at $z \simeq 6$ (Sun et al. 2024).

3.5. Extraction of *Virgil*'s photometry

After having removed the lower redshift interloper from all the 31 available HST (ACS and WFC3) and JWST (NIRCcam and MIRI) bands, we extract *Virgil*'s photometry in the wavelength range 0.4–25 μm

with SEP (Barbary et al. 2017), a PYTHON version of SExtractor (Bertin & Arnouts 1996b). However, at the longest MIRI wavelengths ($> 15 \mu\text{m}$), the available imaging is too shallow to detect *Virgil*. Also after stacking together all the different MIRI bands available above 15 μm (i.e. F1800W, F2100W, F2550W) we fail to detect our target. Hence, above 15 μm we make use of the 3σ upper limits on the flux density.

At shorter wavelengths ($\leq 15 \mu\text{m}$), we extract *Virgil* photometry within Kron apertures (Kron 1980), allowing the Kron parameters to vary from filter to filter and replicating standard SExtractor settings, i.e. $K = 2.5$ and a minimum radius $r = 1''.75$. Then, we correct the extracted fluxes to account for the missing flux outside the Kron aperture. To do so, we compute the fraction of the missing light outside the Kron apertures (e.g. Whitaker et al. 2011; Weaver et al. 2023; Kokorev et al. 2024) in comparison to the curve of growth of the different PSFs. For the JWST filters, we employ the PSF models by WEBBPSF (Perrin et al. 2014), while for HST we resort to the curve of encircled energy reported by STScI⁷. We finally correct for Galactic extinction. Following Iani et al. (2024), we obtain the Galactic extinction corrections assuming the colour excess reported on the IRSA webpage⁸ at *Virgil*'s coordinates ($E(B - V) = 0.008$, Schlafly & Finkbeiner 2011) and, for all filters with an effective wavelength $\lambda_{\text{eff}} < 1.25 \mu\text{m}$, applying the Fitzpatrick (1999) extinction law, while at longer wavelengths ($1.25 \leq \lambda_{\text{eff}} < 8 \mu\text{m}$), resorting to the Indebetouw et al. (2005) law. The correction factors for Galactic extinction are, however, quite negligible ($< 3\%$).

As in the case of SExtractor (Sonnott et al. 2013), SEP tends to underestimate the errors on the fluxes. To derive more reliable errors, we estimate them drawing in each filter 1000 random Kron apertures on the sky region around *Virgil* ($6'' \times 6''$) and, after having masked all the close-by sources, measuring their fluxes. We then take the standard deviation of all the different measurements taking into account effects of pixel correlation (Fruchter & Hook 2002). Similarly to the fluxes, we also correct the errors to total flux and Galactic extinction. Finally, we impose as a minimum error on the photometry a value of 0.05 mag for all bands. We present *Virgil*'s photometry in Table 1.

In addition to HST and JWST imaging, we search for detection of *Virgil* at (sub-)millimeter wavelengths

⁷ The encircled energy curves are available at <https://www.stsci.edu/hst/instrumentation/>;

⁸ <https://irsa.ipac.caltech.edu/applications/DUST/>;

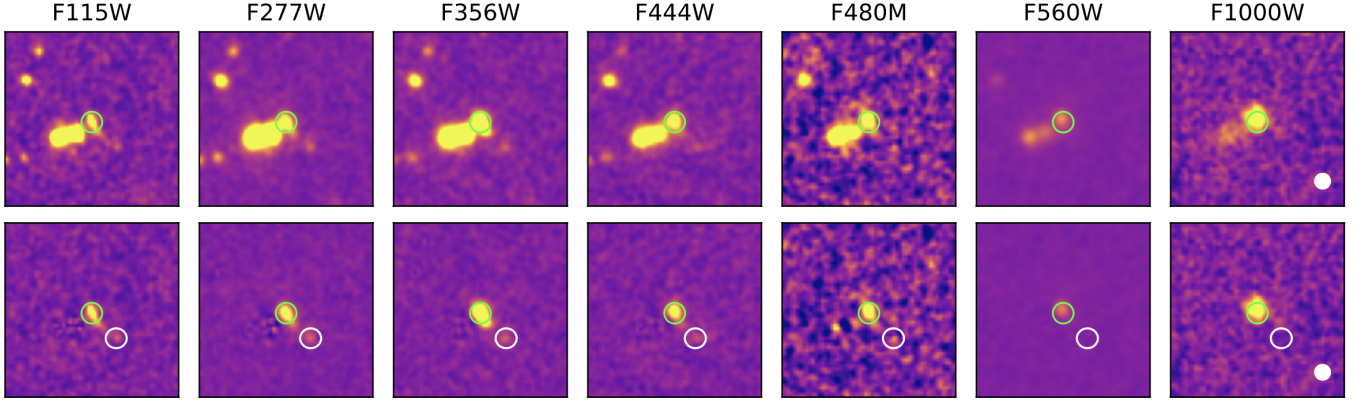


Figure 3. **Top panels:** cutouts ($3''.4 \times 3''.4$) of *Virgil* from NIRCcam (F115W, F277W, F356W, F444W, F480M) and MIRI (F560W, F1000W) imaging. We highlight the position of *Virgil* with a green circle ($0''.2$ radius). The south-eastern component that gets dimmer at longer wavelengths is the LAE contaminant at $z = 4.77$ (Bacon et al. 2023a; Matthee et al. 2022). The white circle at the bottom right corner of the F1000W cutouts is representative of the MIRI $10\mu\text{m}$ PSF (FWHM $\simeq 0''.33$). **Bottom panels:** same cutouts after modeling and subtracting the contaminant at $z = 4.77$ and close-by sources. The white circle ($0''.2$ radius) highlights the position of *Beatrix*.

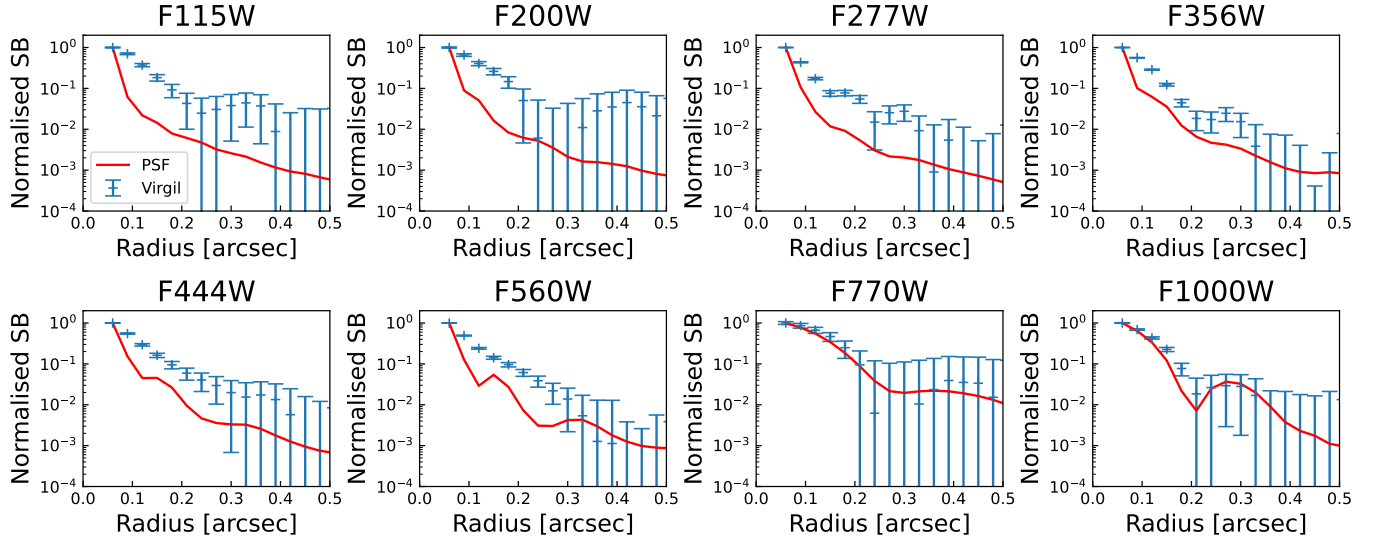


Figure 4. Surface brightness (SB) profiles of *Virgil* at different NIRCcam and MIRI wavelengths (blue errorbars). The surface brightness profiles are normalised at *Virgil*'s peak. The red curves show the JWST PSF trend for the different instruments and filters.

leveraging on the available deep ASPECS ALMA dust continuum imaging at 1.2 and 3.0 mm. By carefully inspecting these maps, *Virgil* is not detected at either wavelengths, see Figure 5. This finding implies 3σ upper limits on the flux density at 1.2 mm and 3.0 mm of $27.9 \mu\text{Jy}$ and $4.2 \mu\text{Jy}$, respectively (assuming it is an unresolved point-like source; Boogaard et al. 2023; Pérez-González et al. 2024b).

To assess the quality of our photometry on the images cleaned for the contaminant, we decide to test if, by running Spectral Energy Distribution (SED) fitting codes on our photometry (up to the reddest NIRCcam

band, i.e. F480M), we retrieve photometric redshifts in agreement with the spectroscopic redshift from MUSE. To this purpose, we employ both EAZY (Brammer et al. 2008) and CIGALE (Burgarella et al. 2005; Noll et al. 2009; Boquien et al. 2019). According to both codes, the probability distribution of the photometric redshifts (PDZ) is uniquely determined (one single narrow peak) to be at 6.61 ± 0.02 (EAZY) and 6.68 ± 0.23 (CIGALE). Overall, we find a very good agreement with the spectroscopic estimate from MUSE.

In addition to *Virgil*, we extract the photometry for *Beatrix* following the same methodology as presented

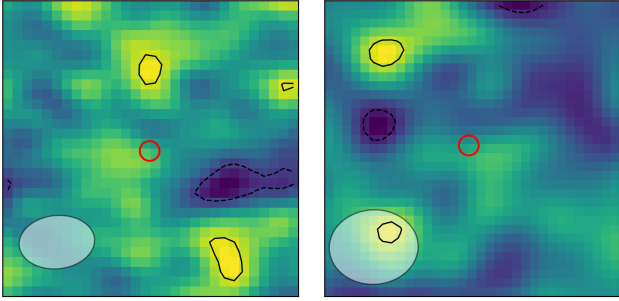


Figure 5. ALMA cutouts ($6'' \times 6''$) at 1.2 mm (band 6) and 3.0 mm (band 3) from ASPECS. Contours are drawn at 1σ intervals starting at $\pm 2\sigma$ (dashed lines show negative contours). The source position is indicated with a $0.2''$ radius circle. The beam size is shown in the bottom left corner. The source is not detected at either wavelength.

above. Our aim is to understand if we can assess the redshift of this object and discern if it is part of *Virgil* (clump) or a source at a different redshift. Due to the faintness of the source, however, we can only detect *Beatrix* in few HST and JWST/NIRCam bands. On the derived photometry, we run both EAZY and CIGALE. Both codes return a multi-peaked PDZ. Interestingly, one of the peaks falls at *Virgil*'s redshift and another one corresponds to the redshift of the contaminant LAE at $z \simeq 4.77$. The other peaks, however, suggest even lower redshift solutions ($z_{phot} < 2$). Due to the limited dataset available and the fact that we are not sure about its redshift, we do not further investigate this object.

3.6. Possible galaxy - galaxy lensing effect on *Virgil*

Due to the closeness of the contaminant to *Virgil* and the extended and stretched morphology of our target, we investigate if *Virgil* could be affected by a galaxy - galaxy lensing effect (e.g. Matthee et al. 2017). To estimate the magnification of *Virgil* by the foreground LAE we resort to the usage of the LENSTRONOMY software (Birrer & Amara 2018). The measured stellar masses of the two components of the foreground LAE are $M_* \simeq 10^{8.3} M_\odot$ and $10^{8.6} M_\odot$ (Eisenstein et al. 2023a) for the objects located $0''.4$ and $0''.7$ from *Virgil*, respectively. The two components are located $0''.32$, or about 2.1 pkpc from each other at $z = 4.77$. The separations involved are sufficiently large that the lensing model is mostly unaffected by assumptions on the mass profile of the lensing galaxies; the Einstein radius is ~ 5 mas using a point-mass approximation, and $\lesssim 20$ mas when assuming extended mass distributions (maximized using an ellipsoid configuration). This configuration results in a magnification $< 5\%$ of *Virgil* even under extreme assumptions for the total-mass-to-stellar-mass ratios of 10 for both

Table 1. Photometry of *Virgil*

Instrument	Filter	f_ν	$\text{err}(f_\nu)$
		[nJy]	[nJy]
JWST/NIRCam	F090W	12.86	2.25
HST/ACS_WFC	F850LP	3.38	2.70
HST/WFC3_IR	F105W	22.07	1.95
JWST/NIRCam	F115W	30.54	2.00
HST/WFC3_IR	F125W	27.06	2.51
HST/WFC3_IR	F140W	22.90	2.59
JWST/NIRCam	F150W	28.92	1.85
HST/WFC3_IR	F160W	28.52	2.82
JWST/NIRCam	F182M	24.63	2.65
JWST/NIRCam	F200W	30.32	2.04
JWST/NIRCam	F210M	36.70	3.10
JWST/NIRCam	F277W	40.11	1.85
JWST/NIRCam	F335M	38.88	2.26
JWST/NIRCam	F356W	93.84	4.32
JWST/NIRCam	F410M	37.01	1.89
JWST/NIRCam	F430M	37.79	4.80
JWST/NIRCam	F444W	49.33	2.27
JWST/NIRCam	F460M	46.99	6.25
JWST/NIRCam	F480M	67.58	7.91
JWST/MIRI	F560W	107.70	3.03
JWST/MIRI	F770W	248.20	30.13
JWST/MIRI	F1000W	399.10	23.79
JWST/MIRI	F1280W	382.70	161.10
JWST/MIRI	F1500W	379.50	296.20

NOTE—In the above table, we report the photometry of *Virgil* as extracted after the modeling of the $z = 4.77$ LAE contaminant (see §3.3). The table is limited to only those bands where it was possible to detect *Virgil*.

foreground galaxies. Due to the minimum value of the retrieved magnification, we do not consider corrections for lensing in the following analysis.

3.7. Spectral energy distribution analysis of *Virgil*

After having extracted its decontaminated photometry, we try to reproduce *Virgil*'s observed SED with different SED fitting codes, namely, CIGALE, BAGPIPES (Carnall et al. 2018), PROSPECTOR (Johnson et al. 2021), and SYNTHESIZER-AGN (Pérez-González et al. 2003, 2008, 2024a). Due to *Virgil*'s red F444W - F1000W color, we decide to run the codes both excluding and considering the presence of an AGN.

We first employ CIGALE assuming a delayed exponentially declining SFH (delayed- τ model) modelled

with two stellar populations. We adopt the BC03 stellar populations models with both solar and sub-solar metallicity ($Z = 0.2Z_{\odot}$), and the Chabrier IMF. We include nebular continuum and emission lines using solar and sub-solar metallicity and allowing the electron density n_e and ionisation parameter U to assume values of $n_e = 10, 100, 1000 \text{ cm}^{-3}$ and $\log_{10}(U) = -2, -1$, respectively. For the dust attenuation, we adopt C00 while for the far-IR emission, we resort to the Draine et al. (2014) models. We add the AGN emission using the SKIRTOR models (Stalevski et al. 2012, 2016) following the initial parameters suggested by Yang et al. (2023) but allowing for the presence of both a Type I (unobscured) and 2 (obscured) AGN.

As a second SED-fitting code, we run BAGPIPES, a stellar population synthesis modeling package built on the BC03 spectral library with the 2016 version of the MILES library (Falc3n-Barroso et al. 2011). The code uses a Kroupa (2001) IMF, adopts the C00 dust attenuation curve and includes nebular emission lines. The ionisation parameter $\log_{10}(U)$ is set to vary between $(-4, -2)$. The SFH is set to two components delayed- τ model and we included an AGN component as in Carnall et al. (2023).

We also fit the photometry with PROSPECTOR, adopting the setup described in detail in Langeroodi et al. (2023) and Langeroodi & Hjorth (2023b). In brief, we use 5 temporal bins to model the star-formation history non-parametrically while applying the continuity prior from Leja et al. (2019). The nebular emission is modelled using the CLOUDY (Chatzikos et al. 2023) templates compiled in Byler et al. (2017), while the gas-phase metallicity, stellar metallicity, and ionization parameters are modelled as free parameters. We model the dust attenuation using the two-component model of Kriek & Conroy (2013), where one component affects the entire galaxy and the other models the additional reddening at the birthplace of young stars.

Finally, we run SYNTHESIZER-AGN. The code assumes that the SED can be modelled with a composite stellar population (P3rez-Gonz3lez et al. 2003, 2008) and AGN emission coming from the accretion disk and the dusty torus (P3rez-Gonz3lez et al. 2024a). The stellar emission includes a young and a more evolved star formation event, each one described by a delayed exponential function with timescales between 1 Myr and 1 Gyr, and with ages from 1 Myr up to the age of the Universe at the redshift of the source. The attenuation of the emission from each stellar population is independent and described by the C00 law, with $A(V)$ values ranging from 0 to 10 mag for each population, considered to have completely independent attenuation. The

stellar emission is described by the BC03 models, assuming a Chabrier IMF with stellar mass limits between 0.1 and 100 M_{\odot} , and the nebular emission is also considered (P3rez-Gonz3lez et al. 2003). The AGN emission is modelled with a QSO average spectrum (Vanden Berk et al. 2001; Glikman et al. 2006). The dust emission from the AGN is modelled with the self-consistent templates of AGN tori presented in Siebenmorgen et al. (2015).

We present and discuss the results derived from the different SED-fitting codes in §4.

4. DISCUSSION

4.1. *Virgil's properties without MIRI*

As a first step, we decide to investigate *Virgil's* properties based on its HST and JWST/NIRCam photometry only, i.e. limiting our study to wavelengths $< 5 \mu\text{m}$.

The SED of *Virgil* reveals a rest-frame blue UV continuum. Following Castellano et al. (2012), we estimate a slope of $\beta = -2.3 \pm 0.2$ and an absolute UV magnitude at 1500 Å $M(\text{UV}) = -19.12 \pm 0.06 \text{ mag}$. Both parameters are well in agreement with what was found for other LAEs at similar redshifts (Iani et al. 2024) and suggest negligible effects due to dust extinction (e.g., Meurer et al. 1999). If we convert the $M(\text{UV})$ into SFR following the prescription by Kennicutt & Evans (2012), we find an $\text{SFR}(\text{UV}) \simeq 1.7 M_{\odot} \text{ yr}^{-1}$ (not corrected for dust extinction).

At optical wavelengths, the clear excess in the F356W band ($F335M - F356W = 0.96 \pm 0.08$) is the consequence of a strong $\text{H}\beta + [\text{O III}]\lambda\lambda 4959, 5007$ ($[\text{O III}]$, hereafter) emission line complex. If we assume the continuum below $\text{H}\beta + [\text{O III}]$ as the average value between the F356W adjoining filters F335M and F410M and apply the prescriptions by M3rmo1-Queralt3 et al. 2016, we can convert the photometric excess in F356W into the rest-frame equivalent width EW_0 of the line complex. From our photometry, we estimate $\text{EW}_0(\text{H}\beta + [\text{O III}]) \simeq 560 \text{ \AA}$. This value is in good agreement with recent literature for emitters at $z \gtrsim 6$ (Prieto-Lyon et al. 2023; Rinaldi et al. 2023a). We highlight that an increase in flux is also observed in the NIRCam longest wavelength filter, e.g. $F460M - F480M = 0.39 \pm 0.19$. At *Virgil's* redshift (i.e., $z_{\text{spec}} = 6.6312 \pm 0.0019$) and without the information coming from the MIRI imaging, this flux excess could be easily ascribed to the $\text{H}\alpha$ emission line entering the F480M filter. In fact, medium band filters are known for their heightened sensitivity to strong emission lines (e.g. Papovich et al. 2023; Rinaldi et al. 2023a; Caputi et al. 2023). Hence, by limiting the analysis of *Virgil* at rest-frame wavelengths $\leq 0.65 \mu\text{m}$, the observed SED would indicate that *Virgil* is simply a strong line emitter, as typically found

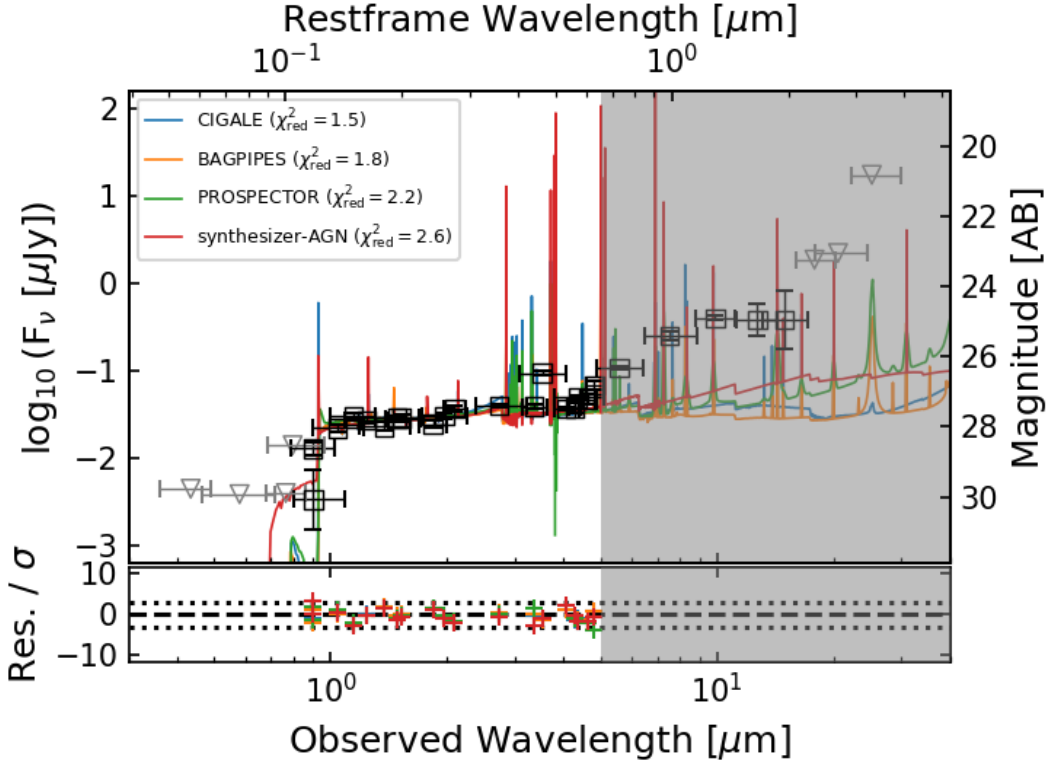


Figure 6. *Virgil*'s photometry (black open squares and gray triangles for the upper-limits) and best-fit models obtained with the SED fitting codes CIGALE (blue) and BAGPIPES (orange) when limiting the analysis to the HST + JWST/NIRCam coverage, i.e. up to about $5 \mu\text{m}$ (rest-frame $0.65 \mu\text{m}$). The bottom panel shows the ratio between the residuals (i.e. the synthetic minus the observed photometry) and the photometric error σ for all the available bands. The dotted lines are indicative of residuals equal to $\pm 3\sigma$.

for LAEs (e.g., Ouchi et al. 2020). This is also confirmed by our runs with SED fitting codes limited to the available photometry below the MIRI/F560W imaging. In this case, all the codes model *Virgil* as a young (≤ 100 Myr) star-forming ($\text{SFR} = 1 - 2 M_{\odot} \text{ yr}^{-1}$) low-mass galaxy ($M_{\star} \simeq 10^{8.0-8.5} M_{\odot}$) with low dust content ($A_V \leq 0.8$ mag), see Figure 6.

4.2. *Virgil*'s full SED

The distinctive feature of *Virgil* lies in its pronounced increase in brightness beyond $0.6 \mu\text{m}$ rest-frame ($4.8 \mu\text{m}$ observed-frame), leading to a notable upturn in its SED at near-IR wavelengths. While the increase in the reddest NIRCam medium band filters F460M and F480M could be potentially caused by the presence of a strong $\text{H}\alpha + [\text{N II}]\lambda\lambda 6548, 6584$ line complex (e.g., Papovich et al. 2023), the steep rising MIRI SED from $0.7 \mu\text{m}$ (F560W) up to $1.3 \mu\text{m}$ (F1000W) rest-frame cannot be solely due to strong emission lines. In fact, although at $z = 6.6312$ the Paschen- β ($\text{Pa}\beta$) emission line enters the F1000W band, atomic physics predicts that the

$\text{Pa}\beta$ intensity is about 1/20 of the $\text{H}\alpha$ line (assuming case B recombination, e.g. Osterbrock & Ferland 2006). Besides, F1000W is a very wide band, with an effective width of about 17000 \AA . Hence, for a galaxy at *Virgil*'s redshift, already an excess of 0.1 mag in F1000W would imply a rest-frame equivalent width for the emission line of about 200 \AA , about 1/3 of what we estimate for the $\text{H}\beta + [\text{O III}]$ complex. Based on our best SED fitting models performed considering only stellar populations (see Figure 7), we would expect an excess of 0.5 mag with respect to the models' continuum in F1000W, thus suggesting a rest-frame equivalent width of about 820 \AA ($\approx 1.5 \times \text{EW}_0(\text{H}\beta + [\text{O III}])$), thus implying an unrealistically strong $\text{Pa}\beta$ line. A similar reasoning can be applied to *Virgil*'s detection ($\text{S/N} \approx 5$) in F770W (effective width of about 18300 \AA), with a flux ≈ 2.5 times higher than what we detect in F560W ($\text{F560W} - \text{F770W} = 1.01 \pm 0.23$).

When considering all the MIRI photometry available, our SED fitting implementing only stellar populations (see Table 2), in general, struggles to reproduce *Virgil*'s

overall SED and behaviour at the MIRI wavelengths. The only code that can reproduce *Virgil's* photometry and its red MIRI slope with solely stellar populations is SYNTHESIZER-AGN ($\chi_{red}^2 = 6.9$) thanks to a combination of two sub-solar ($Z \simeq 0.4Z_{\odot}$) young populations (6, 26 Myr old) with very different extinctions ($A_V = 0.5, 4.0$ mag) and combined with a very strong contribution from the nebular continuum, see Figure 7 (top panel). Due to the presence of the older stellar component, the total mass of *Virgil* retrieved by SYNTHESIZER-AGN is $M_{\star} = 10^{9.7 \pm 0.1} M_{\odot}$. This solution would suggest a scenario for *Virgil* as a dusty starburst galaxy not too different from what was recently reported for the GN20 galaxy at $z = 4.05$ (e.g., Colina et al. 2023; Bik et al. 2024; Crespo et al. 2024). In this case, the blue and red components of the SED would arise from different parts of the galaxy. The relatively small angular size of *Virgil* together with the coarser MIRI resolution and the presence of the lower redshift contaminant (§3.3) prevent us, however, from further investigating this scenario based on the currently available data.

The flexibility of SYNTHESIZER-AGN in finding such best-fit result is hardly retrievable with the other SED-fitting codes at our disposal and which struggle to return good best-fit models ($\chi_{red}^2 \gtrsim 20$), failing in reproducing the photometry at the MIRI wavelengths. In this context, CIGALE, BAGPIPES and PROSPECTOR find very similar best-fit parameters, i.e. $M_{\star} \simeq 10^9 M_{\odot}$, $SFR \simeq 3 M_{\odot} \text{ yr}^{-1}$, $A_V \leq 0.8$ mag and a mass-weighted age of about 300 Myr.

To improve the best-fit models, we consider adding an AGN component to the fits. In fact, *Virgil's* SED steep rise at the rest-frame near-IR domain of galaxy spectra could be the sign of an AGN dusty torus (e.g. Hickox & Alexander 2018). As a first step, we verify if *Virgil* is an already known AGN in the literature. To this purpose, we look for possible counterparts of *Virgil* in the available AGN catalogues in HUDF based on both observations by Chandra (e.g. Luo et al. 2017; Evans et al. 2020) and XMM-Newton (Ranalli et al. 2013) but find no X-ray counterpart. We also match our catalogue with the one from Lyu et al. (2022) who extended the detection of AGNs in the HUDF by studying galaxies' rest-frame optical to mid-IR emission. We also consider the recent release of the AGN catalogue by Lyu et al. (2024) and based only on MIRI imaging from the SMILES program. In both cases, we find no counterparts for our target.

Overall, we find that all codes prefer the SED solution implementing an AGN to the case of only stellar populations, delivering better quality fits (i.e. lower χ_{red}^2), see Figure 7 (bottom panel) and Table 3. In

this case, the best-fits are provided by SYNTHESIZER-AGN ($\chi_{red}^2 = 5.4$) and CIGALE ($\chi_{red}^2 = 6.9$). For SYNTHESIZER-AGN, the best-fit indicates a total stellar mass $M_{\star} \simeq 10^{8.2} M_{\odot}$ with two young stellar populations: a 1 Myr old stellar population with a metallicity $Z = 0.2 Z_{\odot}$ and $A_V = 0.5$, and a 25 Myr old stellar population of solar metallicity and $A_V = 0.9$. The smaller stellar mass of this run with respect to the no-AGN case is due to the dominant contribution at the NIR wavelengths of the AGN component. In the case of CIGALE, *Virgil's* best-fit has a stellar mass of $M_{\star} \simeq 10^{8.5 \pm 0.2} M_{\odot}$ and is reproduced with a young (3 Myr) and an older (300 Myr) stellar population with solar metallicities and $A_V = 0.8$. Also for CIGALE, the AGN dominates at the longest MIRI wavelengths, see Figure 8.

We further investigate the properties of the AGN in *Virgil* by estimating its bolometric luminosity L_{bol} and supermassive black-hole mass M_{BH} . Following Kaspi et al. (2000), we derive L_{bol} from the monochromatic luminosity at 5100 Å (corrected for dust extinction) $L_{\lambda}(5100\text{Å})$ as $L_{bol} \approx 9 \cdot \lambda \cdot L_{\lambda}(5100\text{Å})$. In the case of *Virgil*, we obtain $L_{bol} = (8.4 - 11.1) \times 10^{44} \text{ erg s}^{-1}$. By comparing the AGN bolometric luminosity to the Eddington luminosity L_{Edd} (Eddington 1926), we infer an Eddington ratio $\lambda_{Edd} (= L_{bol}/L_{Edd})$ about 0.13-0.15. Finally, we also derive M_{BH} since $M_{BH} \propto [\lambda \cdot L_{\lambda}(5100\text{Å})]^{0.5 \pm 0.1}$ (Kaspi et al. 2000). The range of values we obtain for the mass of the supermassive black hole of our target is $M_{BH} = (4 - 7) \times 10^7 M_{\odot}$. These estimates are in good agreement with the values of bolometric luminosity of reddened AGNs at $z > 4$ studied with JWST (Greene et al. 2024; Furtak et al. 2024; Kokorev et al. 2023; Matthee et al. 2024).

4.3. *Virgil*, a photometrical analogue to LRDs?

Overall, the flat rest-frame UV and the red NIR colors of *Virgil* revealed by our multi-wavelength dataset (HST, JWST NIRCам and MIRI) are similar to the “v-shaped” SED (in the $\lambda - f_{\lambda}$ plane) of the recently discovered population of LRDs (e.g. Labbe et al. 2023; Furtak et al. 2023b; Kokorev et al. 2024; Pérez-González et al. 2024b; Akins et al. 2024; Matthee et al. 2024). In fact, *Virgil's* photometry complies with most of the color criteria used to characterise LRDs at $z > 6$ reported by Kokorev et al. (2024). In particular, for *Virgil* we find:

- F150W - F200W = 0.05 ± 0.10 (< 0.8);
- F277W - F356W = 0.92 ± 0.07 (> 0.6);

Table 2. Stellar SED properties of *Virgil* - only stars

Code	χ_{red}^2	$\log_{10}(M_{\star})$ $\log_{10}([M_{\odot}])$	$A_{V,\text{main}}$ [mag]	Age_{main} [Myr]	$A_{V,\text{young}}$ [mag]	$\text{Age}_{\text{young}}$ [Myr]	$\text{Age}_{\text{mass-weighted}}$ [Myr]	$\text{SFR}_{100\text{Myr}}$ [$M_{\odot} \text{ yr}^{-1}$]
SYNTHESIZER-AGN	6.5	9.71 ± 0.10	4.00 ± 0.1	26 ± 4	0.50 ± 0.01	6 ± 1	32^{+9}_{-7}	-
CIGALE	19.4	8.95 ± 0.08	0.81 ± 0.04	304 ± 223	-	3 ± 1	275 ± 104	2.60 ± 0.87
BAGPIPES	20.6	$8.74^{+0.38}_{-0.12}$	$0.73^{+0.05}_{-0.09}$	720^{+70}_{-230}	-	20^{+2}_{-1}	220^{+370}_{-130}	$3.42^{+0.67}_{-1.35}$
PROSPECTOR	25.1	$9.01^{+0.03}_{-0.16}$	$0.12^{+0.02}_{-0.01}$	-	-	-	367^{+50}_{-80}	$2.53^{+0.51}_{-1.90}$

NOTE—In the above table, we report the main physical properties of *Virgil* as derived from the different SED fitting codes adopted in our study: SYNTHESIZER-AGN, CIGALE, BAGPIPES, and PROSPECTOR. In this table, we present the results derived when considering only the contribution of stellar populations to the overall *Virgil*'s SED. Specifically, we report the logarithm of the stellar mass $\log_{10}(M_{\star})$, the extinction of the main stellar component $A_{V,\text{main}}$ and its age Age_{main} , the extinction of the young stellar component $A_{V,\text{young}}$ and its age $\text{Age}_{\text{young}}$, the mass-weighted age of the overall galaxy $\text{Age}_{\text{mass-weighted}}$ and its average star formation rate over the last 100 Myr $\text{SFR}_{100\text{Myr}}$. We leave an empty entry for parameters where the codes do not provide an estimate.

Table 3. Stellar SED properties of *Virgil* - stars & AGN

Code	χ_{red}^2	$\log_{10}(M_{\star})$ $\log_{10}([M_{\odot}])$	$A_{V,\text{main}}$ [mag]	Age_{main} [Myr]	$A_{V,\text{young}}$ [mag]	$\text{Age}_{\text{young}}$ [Myr]	$\text{Age}_{\text{mass-weighted}}$ [Myr]	$\text{SFR}_{100\text{Myr}}$ [$M_{\odot} \text{ yr}^{-1}$]
SYNTHESIZER-AGN	5.4	8.19 ± 0.07	0.90 ± 0.10	2.5 ± 0.5	0.46 ± 0.03	1 ± 0.5	$0.8^{+0.8}_{-0.2}$	-
CIGALE	6.9	8.50 ± 0.02	0.83 ± 0.04	662 ± 230	-	1.5 ± 0.5	309 ± 121	0.88 ± 0.04
BAGPIPES	12.1	$10.25^{+0.04}_{-0.05}$	$3.57^{+0.18}_{-0.17}$	790^{+20}_{-30}	-	260^{+20}_{-60}	640^{+20}_{-110}	-
PROSPECTOR	23.4	$8.77^{+0.06}_{-0.11}$	$0.11^{+0.01}_{-0.02}$	-	-	-	284^{+100}_{-70}	$2.50^{+0.53}_{-1.75}$

NOTE—As in Table 2, we report the main physical properties of *Virgil* as derived from the different SED fitting codes adopted in our study. In this table, we present the results derived when adding to the contribution of stellar populations also an AGN component.

- F277W - F444W = 0.22 ± 0.07 (> 0.7);
- F115W - F200W = -0.01 ± 0.10 (> -0.5);

where we report within parentheses the color criteria from Kokorev et al. (2024) to select objects with a “v-shaped” SED while minimising the possible contamination from Brown Dwarfs (condition on F115W - F200W). *Virgil*'s photometry complies with all the LRDs colors criteria except for a bluer F277W - F444W color. The bluer F277W - F444W color could be due to the filter placements relative to the nebular lines. At *Virgil*'s redshift, the F444W filter covers the wavelength range between [O III] and $\text{H}\alpha$ ([O III] and $\text{H}\alpha$ fall at observed wavelengths where the NIRCcam F444W filter transmissivity drops below 5%), placing it in a low-flux region, thus possibly resulting in a bluer color. In fact, when replacing F444W with the adjoining MIRI filter F560W, *Virgil* displays a very red F277W - F560W color, i.e. F277W - F560W = 1.10 ± 0.06 .

We also highlight that at rest-frame UV wavelengths, *Virgil* well complies with the Brown Dwarfs rejection criteria from Kokorev et al. (2024) but, in principle, not with the F150W - F200W color criterion of Langeroodi & Hjorth (2023a), who found that objects respecting the above criteria but having F150W - F200W < 0.25 are typically Brown Dwarfs. In this regard, we highlight that it is *Virgil*'s F277W - F444W color that brings our target outside the area of the F277W - F444W vs F150W - F200W diagram populated by the Brown Dwarf models (see Figure 13 of Langeroodi & Hjorth 2023a). In addition, the extended morphology of *Virgil* further discards the hypothesis of our target being a Brown Dwarf.

We also compare *Virgil*'s photometry to the stacked average trend recently found for 20 MIRI-detected LRDs in the HUDF (Pérez-González et al. 2024a), see Figure 9. We find an overall good agreement ($\chi_{\text{red}}^2 = 8.9$) between the shape of our photometry and the observed trend of MIRI-detected LRDs. We also find agreement with the

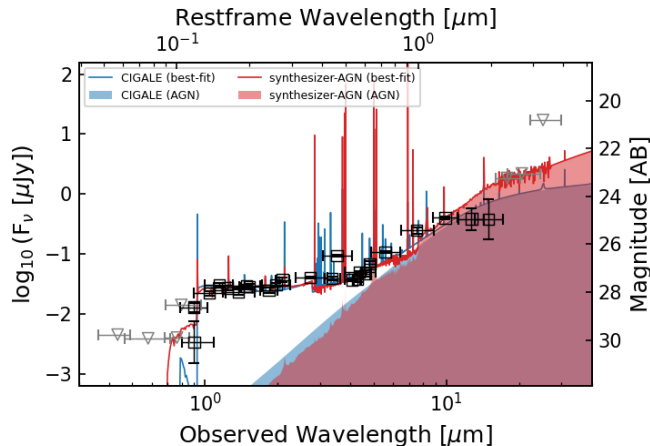


Figure 8. Decomposition of the AGN component from *Virgil*'s photometry (black open squares and gray triangles for the upper-limits) for the best-fit models obtained with the SED fitting codes CIGALE (blue) and SYNTHESIZER-AGN (red).

recently reported trend of 500 LRDs in the COSMOS-Webb field (Akins et al. 2024).

Interestingly, we also note that the non-detection of *Virgil* at the X-ray wavelengths (§4.2) is consistent with what has been recently found for LRDs (Ananna et al. 2024).

Despite their photometric similarities, what distinguishes *Virgil* from the LRDs is its size. In fact, the estimate of the compactness parameter $c = f(D = 0''.4)/f(D = 0''.2)$ performed on the F444W image after the removal of the close-by LAE contaminant (see §3.3) gives $c_{F444W} = 2.0$ that does not satisfy the LRDs compactness requirement, i.e. $c_{F444W} < 1.7$.

The photometric similarities, despite not fully meeting the LRDs' compactness/morphological criteria, raise the question of whether *Virgil* could be the first reported LRD where the host galaxy is detectable at the bluest wavelengths. If so, LRDs might represent the compact branch of a larger, yet undiscovered, AGN population.

Once again, we highlight the fundamental role played by the MIRI dataset. Without MIRI imaging, a classification of *Virgil* as a "v-shaped" object would have not been possible since two requirements (F277W - F444W color and compactness) for the selection of LRDs would have not been satisfied with only NIRCcam imaging.

4.4. The impact of long-wavelengths MIRI filters

A final interesting remark comes from the information that we can obtain thanks to the presence of the longest MIRI wavelengths (i.e. F1280W, F1500W). Despite the shallower depth of the available imaging above 10 μm , we find that the steep rise observed up to F1000W could

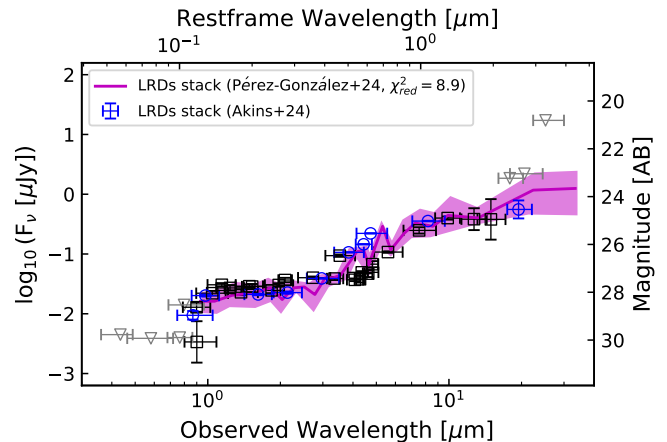


Figure 9. *Virgil*'s photometry (black open squares and gray open triangles for the 3σ upper-limits) and the average observed SED of MIRI-detected LRDs (in magenta) found in the HUDF and reported by Pérez-González et al. (2024a). The blue photometric points are from the average SED of 500 LRDs detected in COSMOS-Webb (Akins et al. 2024).

tend to flatten at longer wavelengths (above the rest-frame 1.6 μm). Interestingly, this flattening is also reported in the average trend of the MIRI-detected LRDs presented by Pérez-González et al. (2024a). We retrieve an estimate of the flux in F1280W (S/N ≈ 2.4) and F1500W (S/N ≈ 1.3) that imply colors of F1000W - F1280W = 0.1 ± 0.2 and F1000W - F1500W = 0.1 ± 0.3 . We underline how, if the flattening trend is confirmed, without any information at these wavelengths the SED codes would tend to prefer models that keep on rising thus over-predicting the flux at the longest wavelengths and overestimating the importance of the AGN dust torus, see Figure 10. This advocates for the importance of conducting deep MIRI imaging above the 10 μm even if challenged by the less sensitivity of the MIRI instrument at such wavelengths.

5. SUMMARY AND CONCLUSIONS

In this paper, we have presented the analysis of *Virgil*, a MIRI extremely red object (MERO) detected with the F1000W filter as part of the MIRI Deep Imaging Survey (MIDIS) observations of the Hubble Ultra Deep Field. *Virgil* is a Ly α emitter at $z = 6.63124 \pm 0.00188$ (VLT/MUSE, Bacon et al. 2023a) showing a red F444W - F1000W = 2.33 ± 0.06 color.

At NIRCcam wavelengths, *Virgil* presents an elongated morphology in the south-west direction and features a tail that ends up in a (faint) compact source (*Beatrice*; $\alpha(\text{J2000.0}) = 03:32:37.8844$ (hours); $\delta(\text{J2000.0}) = -27:47:10.979$). With the current data, it is, however, difficult to assess if this compact object is a clump

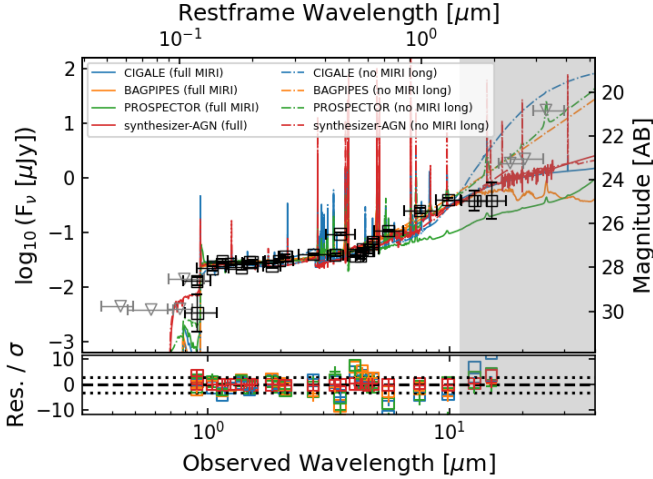


Figure 10. *Virgil*'s photometry (as in the previous panels) and best-fit models obtained with the SED fitting codes CIGALE (blue), BAGPIPES (orange), PROSPECTOR (green) and SYNTHESIZER-AGN (red) in the case of excluding (dashed-dotted lines) and assuming (solid lines) the photometric MIRI information at $> 10 \mu\text{m}$ (gray-shaded area). Similarly, the bottom panel shows the ratio between the residuals and the photometric error for all the available bands when excluding (plus) and assuming (open squares) the MIRI long wavelength filters. The dotted lines are indicative of residuals equal to $\pm 3\sigma$.

of *Virgil*, a clump of a nearby ($\delta = 0''.4 - 0''.7$) foreground ($z \simeq 4.77$) LAE (Matthee et al. 2022), or a different source. By modeling the rest-frame UV-optical morphology of *Virgil* with a Sérsic profile we find a best-fit Sérsic index $n \simeq 0.9$ and an effective radius $r_e \simeq 0.43$ pkpc in agreement with the values recently reported for other galaxies at similar redshifts (Sun et al. 2024). At MIRI wavelengths, the morphology of *Virgil* is dominated by the MIRI PSF.

The extracted photometry of *Virgil* shows a blue UV continuum ($\beta = -2.3 \pm 0.2$), the presence of strong emission lines (flux excess of the F356W band corresponding to the $\text{H}\beta + [\text{O III}]$ complex) and a steep rising SED from 0.7 to $1.3 \mu\text{m}$ (rest-frame). SED fitting models considering only stellar populations struggle to explain *Virgil*'s behaviour at MIRI wavelengths. The best-fit model suggest that *Virgil*'s SED originates from two components: an extremely young (6 Myr) and unobscured stellar population dominating the blue wavelengths, and another young (26 Myr) stellar population strongly affected by extinction ($A_V = 4$ mag) that is responsible for most of the light at red wavelengths. In this case, *Virgil* could be similar to a dusty starburst (e.g., Colina et al. 2023). The small angular size of *Virgil* together

with the coarser MIRI resolution hamper us from deriving if the two populations are located in different parts of the galaxy. All the other codes fail to reproduce the steep and rising MIRI photometry.

Such red rising part of *Virgil*'s SED could hint at the presence of a (dust-obscured) AGN. Despite extensive searches, no AGN counterparts are found in existing multi-wavelength catalogs (Ranalli et al. 2013; Luo et al. 2017; Evans et al. 2020; Lyu et al. 2022, 2024). However, when implementing an AGN contribution to the SED, all the SED-fitting codes adopted deliver significantly improved best-fit models. Assuming the presence of an AGN, we estimate a bolometric luminosity $L_{\text{bol}} = (8.4 - 11.1) \times 10^{44} \text{ erg s}^{-1}$, an Eddington ratio of $\lambda_{\text{Edd}} \approx 0.13 - 0.15$ and an $M_{\text{BH}} = (5 - 7) \times 10^7 M_\odot$. These estimates agree with those reported in the recent literature targeting reddened AGNs at $z > 4$ (Kokorev et al. 2023; Matthee et al. 2024; Furtak et al. 2024).

Virgil's flat rest-frame UV and red NIR colors and, in general, the shape of its SED, remind that of the recently discovered population of LRDs (e.g. Labbe et al. 2023; Kokorev et al. 2024; Pérez-González et al. 2024a), even though its morphology does not satisfy the LRDs' compactness requirement. Also the comparison of *Virgil*'s SED with the recently reported show that our target is a photometric analogue of the population of the LRDs. The extended morphology of *Virgil* could suggest that it is the first LRD for which we can detect the host galaxy.

Despite the richness of the photometric dataset available, deeper MIRI long-wavelength observations in combination with a rest-frame optical and near-infrared spectroscopic follow-up (as demonstrated in recent literature, e.g. Wang et al. 2024; Tacchella et al. 2024; Li et al. 2024) appear to be fundamental to properly assess the nature of *Virgil*.

All in all, our findings show the power of MIRI imaging in unveiling the complexity of this galaxy's nature. For our target, MIRI provides a fundamental piece of information that would be otherwise completely missed without imaging at such long wavelengths. This discovery opens up to the question how many objects like *Virgil* there are in the Universe. If a systematic search for similar objects in deep MIRI surveys would reveal several *Virgil*-like objects and their AGN-nature is confirmed, this discovery could potentially bring us to reassess (once more) the role of AGN to the reionization. In addition to a more general importance of MIRI in the characterisation of galaxy properties, this study also advocates for the importance of conducting deep and extended MIRI surveys at $\lambda > 10 \mu\text{m}$ wavelengths, a regime that results in being crucial in correctly determining the physical properties of galaxies and unveil-

ing their hidden components. In fact, the absence of MIRI long-wavelength photometry (even in the case of upper-limits) biases us to overestimate the contribution of AGN in the SED of such objects.

ACKNOWLEDGMENTS

The authors thank Ryan Cooper, Guang Yang, Vasily Kokorev and Di Wen for useful discussions and comments.

E.I. and K.I.C. acknowledge funding from the Netherlands Research School for Astronomy (NOVA). K.I.C. acknowledges funding from the Dutch Research Council (NWO) through the award of the Vici Grant VI.C.212.036. A.A.-H. acknowledges support from grant PID2021-124665NB-I00 funded by MCIN/AEI/10.13039/501100011033 and by “ERDF A way of making Europe”. P.G.P.-G. acknowledges support from grant PID2022-139567NB-I00 funded by Spanish Ministerio de Ciencia e Innovación MCIN/AEI/10.13039/501100011033, FEDER *Una manera de hacer Europa*. J.A.-M., A.C.-G. and L. Colina, acknowledge support by grant PIB2021-127718NB-100 from the Spanish Ministry of Science and Innovation/State Agency of Research MCIN/AEI/10.13039/501100011033 and by “ERDF A way of making Europe”. L. Colina thanks the support from the Cosmic Dawn Center received during visits to DAWN as international associate. L. Costantin acknowledges support by grants PIB2021-127718NB-100 and PID2022-139567NB-I00 from the Spanish Ministry of Science and Innovation/State Agency of Research MCIN/AEI/10.13039/501100011033 and by “ERDF A way of making Europe”. T.R.G. acknowledges support from the Carlsberg Foundation (grant no CF20-0534). S.G. acknowledges financial support from the Cosmic Dawn Center (DAWN), funded by the Danish National Research Foundation (DNRF) under grant No. 140. This work was supported by research grants (VIL16599, VIL54489) from VILLUM FONDEN. J.P.P. and T.V.T. acknowledge financial support from the UK Science and Technology Facilities Council, and the UK Space Agency.

This work is based on observations made with the NASA/ESA/CSA James Webb Space Telescope. The data were obtained from the Mikulski Archive for Space Telescopes at the Space Telescope Science Institute, which is operated by the Association of Universities for Research in Astronomy, Inc., under NASA contract NAS 5-03127 for JWST. These observations are associated with programs GO #1963, GO #1895 and GTO #1283. The authors acknowledge the team led by coPIs C. Williams, M. Maseda and S. Tacchella, and PI P. Oesch,

for developing their respective observing programs with a zero-exclusive-access period. Also based on observations made with the NASA/ESA Hubble Space Telescope obtained from the Space Telescope Science Institute, which is operated by the Association of Universities for Research in Astronomy, Inc., under NASA contract NAS 5-26555. The work presented here is the effort of the entire MIRI team and the enthusiasm within the MIRI partnership is a significant factor in its success. MIRI draws on the scientific and technical expertise of the following organisations: Ames Research Center, USA; Airbus Defence and Space, UK; CEA-Irfu, Saclay, France; Centre Spatial de Liège, Belgium; Consejo Superior de Investigaciones Científicas, Spain; Carl Zeiss Optronics, Germany; Chalmers University of Technology, Sweden; Danish Space Research Institute, Denmark; Dublin Institute for Advanced Studies, Ireland; European Space Agency, Netherlands; ETCA, Belgium; ETH Zurich, Switzerland; Goddard Space Flight Center, USA; Institute d’Astrophysique Spatiale, France; Instituto Nacional de Técnica Aeroespacial, Spain; Institute for Astronomy, Edinburgh, UK; Jet Propulsion Laboratory, USA; Laboratoire d’Astrophysique de Marseille (LAM), France; Leiden University, Netherlands; Lockheed Advanced Technology Center (USA); NOVA Opt-IR group at Dwingeloo, Netherlands; Northrop Grumman, USA; Max-Planck Institut für Astronomie (MPIA), Heidelberg, Germany; Laboratoire d’Etudes Spatiales et d’Instrumentation en Astrophysique (LESIA), France; Paul Scherrer Institut, Switzerland; Raytheon Vision Systems, USA; RUAG Aerospace, Switzerland; Rutherford Appleton Laboratory (RAL Space), UK; Space Telescope Science Institute, USA; Toegepast-Natuurwetenschappelijk Onderzoek (TNO-TPD), Netherlands; UK Astronomy Technology Centre, UK; University College London, UK; University of Amsterdam, Netherlands; University of Arizona, USA; University of Cardiff, UK; University of Cologne, Germany; University of Ghent; University of Groningen, Netherlands; University of Leicester, UK; University of Leuven, Belgium; University of Stockholm, Sweden; Utah State University, USA.

For the purpose of open access, the author has applied a Creative Commons Attribution (CC BY) licence to the Author Accepted Manuscript version arising from this submission.

Facilities: VLT, HST, JWST, ALMA.

Software: [ASTROPY](#) (Astropy Collaboration et al. 2013, 2018, 2022), [NUMPY](#) (Harris et al. 2020), [PANDAS](#) (Wes McKinney 2010; pandas development team

2020) PHOTUTILS (Bradley et al. 2022), SCIPY (Virtanen et al. 2020), WEBBPSF (Perrin et al. 2014), SOURCE EXTRACTOR (Bertin & Arnouts 1996b), LENSTRONOMY (Birrer & Amara 2018), SEP (Barbary et al. 2017), LEPHARE (Ilbert et al. 2006; Arnouts & Ilbert 2011), EAZY

(Brammer et al. 2008), BAGPIPES (Carnall et al. 2018), CIGALE (Burgarella et al. 2005; Noll et al. 2009; Boquien et al. 2019), PROSPECTOR (Johnson et al. 2021), SYNTHESIZER-AGN (Pérez-González et al. 2003, 2008), ASTROPHOT (Stone et al. 2023), TOPCAT (Taylor 2011).

REFERENCES

- Akins, H. B., Casey, C. M., Allen, N., et al. 2023, *ApJ*, 956, 61, doi: [10.3847/1538-4357/acef21](https://doi.org/10.3847/1538-4357/acef21)
- Akins, H. B., Casey, C. M., Lambrides, E., et al. 2024, arXiv e-prints, arXiv:2406.10341, <https://arxiv.org/abs/2406.10341>
- Alcalde Pampliega, B., Pérez-González, P. G., Barro, G., et al. 2019, *ApJ*, 876, 135, doi: [10.3847/1538-4357/ab14f2](https://doi.org/10.3847/1538-4357/ab14f2)
- Álvarez-Márquez, J., Colina, L., Crespo Gómez, A., et al. 2023a, arXiv e-prints, arXiv:2309.06319, doi: [10.48550/arXiv.2309.06319](https://doi.org/10.48550/arXiv.2309.06319)
- . 2023b, arXiv e-prints, arXiv:2309.06319, doi: [10.48550/arXiv.2309.06319](https://doi.org/10.48550/arXiv.2309.06319)
- Ananna, T. T., Bogdán, Á., Kovács, O. E., Natarajan, P., & Hickox, R. C. 2024, arXiv e-prints, arXiv:2404.19010, doi: [10.48550/arXiv.2404.19010](https://doi.org/10.48550/arXiv.2404.19010)
- Arnouts, S., & Ilbert, O. 2011, LePHARE: Photometric Analysis for Redshift Estimate, Astrophysics Source Code Library, record ascl:1108.009
- Astropy Collaboration, Robitaille, T. P., Tollerud, E. J., et al. 2013, *A&A*, 558, A33, doi: [10.1051/0004-6361/201322068](https://doi.org/10.1051/0004-6361/201322068)
- Astropy Collaboration, Price-Whelan, A. M., Sipőcz, B. M., et al. 2018, *AJ*, 156, 123, doi: [10.3847/1538-3881/aabc4f](https://doi.org/10.3847/1538-3881/aabc4f)
- Astropy Collaboration, Price-Whelan, A. M., Lim, P. L., et al. 2022, *apj*, 935, 167, doi: [10.3847/1538-4357/ac7c74](https://doi.org/10.3847/1538-4357/ac7c74)
- Atek, H., Shuntov, M., Furtak, L. J., et al. 2023a, *MNRAS*, 519, 1201, doi: [10.1093/mnras/stac3144](https://doi.org/10.1093/mnras/stac3144)
- Atek, H., Chemerynska, I., Wang, B., et al. 2023b, *MNRAS*, 524, 5486, doi: [10.1093/mnras/stad1998](https://doi.org/10.1093/mnras/stad1998)
- Bacon, R., Accardo, M., Adjali, L., et al. 2010, in *Society of Photo-Optical Instrumentation Engineers (SPIE) Conference Series*, Vol. 7735, *Ground-based and Airborne Instrumentation for Astronomy III*, ed. I. S. McLean, S. K. Ramsay, & H. Takami, 773508, doi: [10.1117/12.856027](https://doi.org/10.1117/12.856027)
- Bacon, R., Conseil, S., Mary, D., et al. 2017, *A&A*, 608, A1, doi: [10.1051/0004-6361/201730833](https://doi.org/10.1051/0004-6361/201730833)
- Bacon, R., Brinchmann, J., Conseil, S., et al. 2023a, *A&A*, 670, A4, doi: [10.1051/0004-6361/202244187](https://doi.org/10.1051/0004-6361/202244187)
- . 2023b, *A&A*, 670, A4, doi: [10.1051/0004-6361/202244187](https://doi.org/10.1051/0004-6361/202244187)
- Bagley, M. B., Pirzkal, N., Finkelstein, S. L., et al. 2024, *ApJL*, 965, L6, doi: [10.3847/2041-8213/ad2f31](https://doi.org/10.3847/2041-8213/ad2f31)
- Barbary, K., Boone, K., Craig, M., Deil, C., & Rose, B. 2017, *kbarbary/sep*: v1.0.2, v1.0.2, Zenodo, doi: [10.5281/zenodo.896928](https://doi.org/10.5281/zenodo.896928)
- Barro, G., Perez-Gonzalez, P. G., Kocevski, D. D., et al. 2023, arXiv e-prints, arXiv:2305.14418, doi: [10.48550/arXiv.2305.14418](https://doi.org/10.48550/arXiv.2305.14418)
- Beckwith, S. V. W., Stiavelli, M., Koekemoer, A. M., et al. 2006, *AJ*, 132, 1729, doi: [10.1086/507302](https://doi.org/10.1086/507302)
- Bertin, E., & Arnouts, S. 1996a, *A&AS*, 117, 393, doi: [10.1051/aas:1996164](https://doi.org/10.1051/aas:1996164)
- . 1996b, *A&AS*, 117, 393, doi: [10.1051/aas:1996164](https://doi.org/10.1051/aas:1996164)
- Bik, A., Álvarez-Márquez, J., Colina, L., et al. 2024, *A&A*, 686, A3, doi: [10.1051/0004-6361/202348845](https://doi.org/10.1051/0004-6361/202348845)
- Birrer, S., & Amara, A. 2018, *Physics of the Dark Universe*, 22, 189, doi: [10.1016/j.dark.2018.11.002](https://doi.org/10.1016/j.dark.2018.11.002)
- Blain, A. W., Smail, I., Ivison, R. J., Kneib, J. P., & Frayer, D. T. 2002, *PhR*, 369, 111, doi: [10.1016/S0370-1573\(02\)00134-5](https://doi.org/10.1016/S0370-1573(02)00134-5)
- Boogaard, L. A., Gillman, S., Melinder, J., et al. 2023, arXiv e-prints, arXiv:2308.16895, doi: [10.48550/arXiv.2308.16895](https://doi.org/10.48550/arXiv.2308.16895)
- Boquien, M., Burgarella, D., Roehlly, Y., et al. 2019, *A&A*, 622, A103, doi: [10.1051/0004-6361/201834156](https://doi.org/10.1051/0004-6361/201834156)
- Bouchet, P., García-Marín, M., Lagage, P. O., et al. 2015, *PASP*, 127, 612, doi: [10.1086/682254](https://doi.org/10.1086/682254)
- Bouwens, R. J., Illingworth, G. D., Oesch, P. A., et al. 2011, *ApJ*, 737, 90, doi: [10.1088/0004-637X/737/2/90](https://doi.org/10.1088/0004-637X/737/2/90)
- Boyett, K., Bunker, A. J., Curtis-Lake, E., et al. 2024, arXiv e-prints, arXiv:2401.16934, doi: [10.48550/arXiv.2401.16934](https://doi.org/10.48550/arXiv.2401.16934)
- Bradley, L., Sipőcz, B., Robitaille, T., et al. 2022, *astropy/photutils*: 1.5.0, 1.5.0, Zenodo, doi: [10.5281/zenodo.6825092](https://doi.org/10.5281/zenodo.6825092)
- Brammer, G. B., van Dokkum, P. G., & Coppi, P. 2008, *ApJ*, 686, 1503, doi: [10.1086/591786](https://doi.org/10.1086/591786)
- Bruzual, G., & Charlot, S. 2003, *MNRAS*, 344, 1000, doi: [10.1046/j.1365-8711.2003.06897.x](https://doi.org/10.1046/j.1365-8711.2003.06897.x)
- Bunker, A. J., Saxena, A., Cameron, A. J., et al. 2023, *A&A*, 677, A88, doi: [10.1051/0004-6361/202346159](https://doi.org/10.1051/0004-6361/202346159)

- Burgarella, D., Buat, V., & Iglesias-Páramo, J. 2005, *MNRAS*, 360, 1413, doi: [10.1111/j.1365-2966.2005.09131.x](https://doi.org/10.1111/j.1365-2966.2005.09131.x)
- Byler, N., Dalcanton, J. J., Conroy, C., & Johnson, B. D. 2017, *ApJ*, 840, 44, doi: [10.3847/1538-4357/aa6c66](https://doi.org/10.3847/1538-4357/aa6c66)
- Calzetti, D., Armus, L., Bohlin, R. C., et al. 2000, *ApJ*, 533, 682, doi: [10.1086/308692](https://doi.org/10.1086/308692)
- Caputi, K. I., Dunlop, J. S., McLure, R. J., & Roche, N. D. 2004, *MNRAS*, 353, 30, doi: [10.1111/j.1365-2966.2004.08044.x](https://doi.org/10.1111/j.1365-2966.2004.08044.x)
- Caputi, K. I., Lagache, G., Yan, L., et al. 2007, *ApJ*, 660, 97, doi: [10.1086/512667](https://doi.org/10.1086/512667)
- Caputi, K. I., Dunlop, J. S., McLure, R. J., et al. 2012, *ApJL*, 750, L20, doi: [10.1088/2041-8205/750/1/L20](https://doi.org/10.1088/2041-8205/750/1/L20)
- Caputi, K. I., Rinaldi, P., Iani, E., et al. 2023, arXiv e-prints, arXiv:2311.12691, doi: [10.48550/arXiv.2311.12691](https://doi.org/10.48550/arXiv.2311.12691)
- Carnall, A. C., McLure, R. J., Dunlop, J. S., & Davé, R. 2018, *MNRAS*, 480, 4379, doi: [10.1093/mnras/sty2169](https://doi.org/10.1093/mnras/sty2169)
- Carnall, A. C., McLure, R. J., Dunlop, J. S., et al. 2023, *Nature*, 619, 716, doi: [10.1038/s41586-023-06158-6](https://doi.org/10.1038/s41586-023-06158-6)
- Casey, C. M., Akins, H. B., Shuntov, M., et al. 2023, arXiv e-prints, arXiv:2308.10932, doi: [10.48550/arXiv.2308.10932](https://doi.org/10.48550/arXiv.2308.10932)
- Castellano, M., Fontana, A., Grazian, A., et al. 2012, *A&A*, 540, A39, doi: [10.1051/0004-6361/201118050](https://doi.org/10.1051/0004-6361/201118050)
- Castellano, M., Napolitano, L., Fontana, A., et al. 2024, arXiv e-prints, arXiv:2403.10238, doi: [10.48550/arXiv.2403.10238](https://doi.org/10.48550/arXiv.2403.10238)
- Chabrier, G. 2003, *PASP*, 115, 763, doi: [10.1086/376392](https://doi.org/10.1086/376392)
- Chapman, S. C., Blain, A. W., Smail, I., & Ivison, R. J. 2005, *ApJ*, 622, 772, doi: [10.1086/428082](https://doi.org/10.1086/428082)
- Chatzikos, M., Bianchi, S., Camilloni, F., et al. 2023, *RMxAA*, 59, 327, doi: [10.22201/ia.01851101p.2023.59.02.12](https://doi.org/10.22201/ia.01851101p.2023.59.02.12)
- Chen, C.-C., Gao, Z.-K., Hsu, Q.-N., et al. 2022, *ApJL*, 939, L7, doi: [10.3847/2041-8213/ac98c6](https://doi.org/10.3847/2041-8213/ac98c6)
- Cheng, C., Huang, J.-S., Smail, I., et al. 2023, *ApJL*, 942, L19, doi: [10.3847/2041-8213/aca9d0](https://doi.org/10.3847/2041-8213/aca9d0)
- Colina, L., Crespo Gómez, A., Álvarez-Márquez, J., et al. 2023, *A&A*, 673, L6, doi: [10.1051/0004-6361/202346535](https://doi.org/10.1051/0004-6361/202346535)
- Crespo, D., González-Nuevo, J., Bonavera, L., Cueli, M. M., & Casas, J. M. 2024, *A&A*, 684, A109, doi: [10.1051/0004-6361/202347426](https://doi.org/10.1051/0004-6361/202347426)
- Curtis-Lake, E., Carniani, S., Cameron, A., et al. 2023, *Nature Astronomy*, 7, 622, doi: [10.1038/s41550-023-01918-w](https://doi.org/10.1038/s41550-023-01918-w)
- Decarli, R., Walter, F., González-López, J., et al. 2019, *ApJ*, 882, 138, doi: [10.3847/1538-4357/ab30fe](https://doi.org/10.3847/1538-4357/ab30fe)
- Decarli, R., Aravena, M., Boogaard, L., et al. 2020, *ApJ*, 902, 110, doi: [10.3847/1538-4357/abaa3b](https://doi.org/10.3847/1538-4357/abaa3b)
- D'Eugenio, F., Cameron, A. J., Scholtz, J., et al. 2024, arXiv e-prints, arXiv:2404.06531, doi: [10.48550/arXiv.2404.06531](https://doi.org/10.48550/arXiv.2404.06531)
- Dey, A., Soifer, B. T., Desai, V., et al. 2008, *ApJ*, 677, 943, doi: [10.1086/529516](https://doi.org/10.1086/529516)
- Dicken, D., García Marín, M., Shivaee, I., et al. 2024, arXiv e-prints, arXiv:2403.16686, doi: [10.48550/arXiv.2403.16686](https://doi.org/10.48550/arXiv.2403.16686)
- Draine, B. T., Aniano, G., Krause, O., et al. 2014, *ApJ*, 780, 172, doi: [10.1088/0004-637X/780/2/172](https://doi.org/10.1088/0004-637X/780/2/172)
- Eddington, A. S. 1926, *The Internal Constitution of the Stars*
- Eisenstein, D. J., Willott, C., Alberts, S., et al. 2023a, arXiv e-prints, arXiv:2306.02465, doi: [10.48550/arXiv.2306.02465](https://doi.org/10.48550/arXiv.2306.02465)
- . 2023b, arXiv e-prints, arXiv:2306.02465, doi: [10.48550/arXiv.2306.02465](https://doi.org/10.48550/arXiv.2306.02465)
- Eisenstein, D. J., Johnson, B. D., Robertson, B., et al. 2023c, arXiv e-prints, arXiv:2310.12340, doi: [10.48550/arXiv.2310.12340](https://doi.org/10.48550/arXiv.2310.12340)
- Elbaz, D., Cesarsky, C. J., Chantal, P., et al. 2002, *A&A*, 384, 848, doi: [10.1051/0004-6361:20020106](https://doi.org/10.1051/0004-6361:20020106)
- Elston, R., Rieke, G. H., & Rieke, M. J. 1988, *ApJL*, 331, L77, doi: [10.1086/185239](https://doi.org/10.1086/185239)
- Evans, I. N., Primini, F. A., Miller, J. B., et al. 2020, in *American Astronomical Society Meeting Abstracts*, Vol. 235, American Astronomical Society Meeting Abstracts #235, 154.05
- Falcón-Barroso, J., Sánchez-Blázquez, P., Vazdekis, A., et al. 2011, *A&A*, 532, A95, doi: [10.1051/0004-6361/201116842](https://doi.org/10.1051/0004-6361/201116842)
- Fazio, G. G., Ashby, M. L. N., Barmby, P., et al. 2004, *ApJS*, 154, 39, doi: [10.1086/422585](https://doi.org/10.1086/422585)
- Fitzpatrick, E. L. 1999, *PASP*, 111, 63, doi: [10.1086/316293](https://doi.org/10.1086/316293)
- Franco, M., Elbaz, D., Béthermin, M., et al. 2018, *A&A*, 620, A152, doi: [10.1051/0004-6361/201832928](https://doi.org/10.1051/0004-6361/201832928)
- Fruchter, A. S., & Hook, R. N. 2002, *PASP*, 114, 144, doi: [10.1086/338393](https://doi.org/10.1086/338393)
- Fujimoto, S., Wang, B., Weaver, J., et al. 2023, arXiv e-prints, arXiv:2308.11609, doi: [10.48550/arXiv.2308.11609](https://doi.org/10.48550/arXiv.2308.11609)
- Furtak, L. J., Labbé, I., Zitrin, A., et al. 2023a, arXiv e-prints, arXiv:2308.05735, doi: [10.48550/arXiv.2308.05735](https://doi.org/10.48550/arXiv.2308.05735)
- Furtak, L. J., Zitrin, A., Plat, A., et al. 2023b, *ApJ*, 952, 142, doi: [10.3847/1538-4357/acdc9d](https://doi.org/10.3847/1538-4357/acdc9d)
- Furtak, L. J., Labbé, I., Zitrin, A., et al. 2024, *Nature*, 628, 57, doi: [10.1038/s41586-024-07184-8](https://doi.org/10.1038/s41586-024-07184-8)

- Galametz, A., Grazian, A., Fontana, A., et al. 2013, *ApJS*, 206, 10, doi: [10.1088/0067-0049/206/2/10](https://doi.org/10.1088/0067-0049/206/2/10)
- Gardner, J. P., Mather, J. C., Abbott, R., et al. 2023, *PASP*, 135, 068001, doi: [10.1088/1538-3873/acd1b5](https://doi.org/10.1088/1538-3873/acd1b5)
- Gillman, S., Gullberg, B., Brammer, G., et al. 2023, *A&A*, 676, A26, doi: [10.1051/0004-6361/202346531](https://doi.org/10.1051/0004-6361/202346531)
- Glikman, E., Helfand, D. J., & White, R. L. 2006, *ApJ*, 640, 579, doi: [10.1086/500098](https://doi.org/10.1086/500098)
- González-López, J., Decarli, R., Pavesi, R., et al. 2019, *ApJ*, 882, 139, doi: [10.3847/1538-4357/ab3105](https://doi.org/10.3847/1538-4357/ab3105)
- González-López, J., Novak, M., Decarli, R., et al. 2020, *ApJ*, 897, 91, doi: [10.3847/1538-4357/ab765b](https://doi.org/10.3847/1538-4357/ab765b)
- Graham, J. R., & Dey, A. 1996, *ApJ*, 471, 720, doi: [10.1086/178000](https://doi.org/10.1086/178000)
- Greene, J. E., Labbe, I., Goulding, A. D., et al. 2024, *ApJ*, 964, 39, doi: [10.3847/1538-4357/ad1e5f](https://doi.org/10.3847/1538-4357/ad1e5f)
- Hamann, F., Zakamska, N. L., Ross, N., et al. 2017, *MNRAS*, 464, 3431, doi: [10.1093/mnras/stw2387](https://doi.org/10.1093/mnras/stw2387)
- Harris, C. R., Millman, K. J., van der Walt, S. J., et al. 2020, *Nature*, 585, 357, doi: [10.1038/s41586-020-2649-2](https://doi.org/10.1038/s41586-020-2649-2)
- Hickox, R. C., & Alexander, D. M. 2018, *ARA&A*, 56, 625, doi: [10.1146/annurev-astro-081817-051803](https://doi.org/10.1146/annurev-astro-081817-051803)
- Hughes, D. H., Serjeant, S., Dunlop, J., et al. 1998, *Nature*, 394, 241, doi: [10.1038/28328](https://doi.org/10.1038/28328)
- Iani, E., Zanella, A., Vernet, J., et al. 2023, *MNRAS*, 518, 5018, doi: [10.1093/mnras/stac3198](https://doi.org/10.1093/mnras/stac3198)
- Iani, E., Caputi, K. I., Rinaldi, P., et al. 2024, *ApJ*, 963, 97, doi: [10.3847/1538-4357/ad15f6](https://doi.org/10.3847/1538-4357/ad15f6)
- Ilbert, O., Arnouts, S., McCracken, H. J., et al. 2006, *A&A*, 457, 841, doi: [10.1051/0004-6361:20065138](https://doi.org/10.1051/0004-6361:20065138)
- Indebetouw, R., Mathis, J. S., Babler, B. L., et al. 2005, *ApJ*, 619, 931, doi: [10.1086/426679](https://doi.org/10.1086/426679)
- Johnson, B. D., Leja, J., Conroy, C., & Speagle, J. S. 2021, *ApJS*, 254, 22, doi: [10.3847/1538-4365/abef67](https://doi.org/10.3847/1538-4365/abef67)
- Kaspi, S., Smith, P. S., Netzer, H., et al. 2000, *ApJ*, 533, 631, doi: [10.1086/308704](https://doi.org/10.1086/308704)
- Kennicutt, R. C., & Evans, N. J. 2012, *ARA&A*, 50, 531, doi: [10.1146/annurev-astro-081811-125610](https://doi.org/10.1146/annurev-astro-081811-125610)
- Killi, M., Watson, D., Brammer, G., et al. 2023, arXiv e-prints, arXiv:2312.03065, doi: [10.48550/arXiv.2312.03065](https://doi.org/10.48550/arXiv.2312.03065)
- Kirkpatrick, A., Yang, G., Le Bail, A., et al. 2023, *ApJL*, 959, L7, doi: [10.3847/2041-8213/ad0b14](https://doi.org/10.3847/2041-8213/ad0b14)
- Kocevski, D. D., Onoue, M., Inayoshi, K., et al. 2023, *ApJL*, 954, L4, doi: [10.3847/2041-8213/ace5a0](https://doi.org/10.3847/2041-8213/ace5a0)
- Kokorev, V., Fujimoto, S., Labbe, I., et al. 2023, *ApJL*, 957, L7, doi: [10.3847/2041-8213/ad037a](https://doi.org/10.3847/2041-8213/ad037a)
- Kokorev, V., Caputi, K. I., Greene, J. E., et al. 2024, arXiv e-prints, arXiv:2401.09981, doi: [10.48550/arXiv.2401.09981](https://doi.org/10.48550/arXiv.2401.09981)
- Kriek, M., & Conroy, C. 2013, *ApJL*, 775, L16, doi: [10.1088/2041-8205/775/1/L16](https://doi.org/10.1088/2041-8205/775/1/L16)
- Kron, R. G. 1980, *ApJS*, 43, 305, doi: [10.1086/190669](https://doi.org/10.1086/190669)
- Kroupa, P. 2001, *MNRAS*, 322, 231, doi: [10.1046/j.1365-8711.2001.04022.x](https://doi.org/10.1046/j.1365-8711.2001.04022.x)
- Labbe, I., Greene, J. E., Bezanson, R., et al. 2023, arXiv e-prints, arXiv:2306.07320, doi: [10.48550/arXiv.2306.07320](https://doi.org/10.48550/arXiv.2306.07320)
- Langeroodi, D., & Hjorth, J. 2023a, *ApJL*, 957, L27, doi: [10.3847/2041-8213/acfeec](https://doi.org/10.3847/2041-8213/acfeec)
- . 2023b, arXiv e-prints, arXiv:2307.06336, doi: [10.48550/arXiv.2307.06336](https://doi.org/10.48550/arXiv.2307.06336)
- Langeroodi, D., Hjorth, J., Chen, W., et al. 2023, *ApJ*, 957, 39, doi: [10.3847/1538-4357/acdbcl](https://doi.org/10.3847/1538-4357/acdbcl)
- Le Floch, E., Papovich, C., Dole, H., et al. 2005, *ApJ*, 632, 169, doi: [10.1086/432789](https://doi.org/10.1086/432789)
- Leja, J., Carnall, A. C., Johnson, B. D., Conroy, C., & Speagle, J. S. 2019, *ApJ*, 876, 3, doi: [10.3847/1538-4357/ab133c](https://doi.org/10.3847/1538-4357/ab133c)
- Li, Y., Leja, J., Johnson, B. D., Tacchella, S., & Naidu, R. P. 2024, arXiv e-prints, arXiv:2404.02333, doi: [10.48550/arXiv.2404.02333](https://doi.org/10.48550/arXiv.2404.02333)
- Luo, B., Brandt, W. N., Xue, Y. Q., et al. 2017, *ApJS*, 228, 2, doi: [10.3847/1538-4365/228/1/2](https://doi.org/10.3847/1538-4365/228/1/2)
- Lyu, J., Alberts, S., Rieke, G. H., & Rujopakarn, W. 2022, *ApJ*, 941, 191, doi: [10.3847/1538-4357/ac9e5d](https://doi.org/10.3847/1538-4357/ac9e5d)
- Lyu, J., Alberts, S., Rieke, G. H., et al. 2023, arXiv e-prints, arXiv:2310.12330, doi: [10.48550/arXiv.2310.12330](https://doi.org/10.48550/arXiv.2310.12330)
- . 2024, *ApJ*, 966, 229, doi: [10.3847/1538-4357/ad3643](https://doi.org/10.3847/1538-4357/ad3643)
- Madau, P., & Dickinson, M. 2014, *ARA&A*, 52, 415, doi: [10.1146/annurev-astro-081811-125615](https://doi.org/10.1146/annurev-astro-081811-125615)
- Magnelli, B., Elbaz, D., Chary, R. R., et al. 2009, *A&A*, 496, 57, doi: [10.1051/0004-6361:200811443](https://doi.org/10.1051/0004-6361:200811443)
- Maiolino, R., Uebler, H., Perna, M., et al. 2023, arXiv e-prints, arXiv:2306.00953, doi: [10.48550/arXiv.2306.00953](https://doi.org/10.48550/arXiv.2306.00953)
- Mármol-Queraltó, E., McLure, R. J., Cullen, F., et al. 2016, *MNRAS*, 460, 3587, doi: [10.1093/mnras/stw1212](https://doi.org/10.1093/mnras/stw1212)
- Matthee, J., Sobral, D., Darvish, B., et al. 2017, *MNRAS*, 472, 772, doi: [10.1093/mnras/stx2061](https://doi.org/10.1093/mnras/stx2061)
- Matthee, J., Feltre, A., Maseda, M., et al. 2022, *A&A*, 660, A10, doi: [10.1051/0004-6361/202142187](https://doi.org/10.1051/0004-6361/202142187)
- Matthee, J., Naidu, R. P., Brammer, G., et al. 2024, *ApJ*, 963, 129, doi: [10.3847/1538-4357/ad2345](https://doi.org/10.3847/1538-4357/ad2345)
- Meurer, G. R., Heckman, T. M., & Calzetti, D. 1999, *ApJ*, 521, 64, doi: [10.1086/307523](https://doi.org/10.1086/307523)
- Moffat, A. F. J. 1969, *A&A*, 3, 455
- Narayanan, D., Dey, A., Hayward, C. C., et al. 2010, *MNRAS*, 407, 1701, doi: [10.1111/j.1365-2966.2010.16997.x](https://doi.org/10.1111/j.1365-2966.2010.16997.x)

- Noll, S., Burgarella, D., Giovannoli, E., et al. 2009, *A&A*, 507, 1793, doi: [10.1051/0004-6361/200912497](https://doi.org/10.1051/0004-6361/200912497)
- Oesch, P. A., Brammer, G., Naidu, R. P., et al. 2023a, *MNRAS*, 525, 2864, doi: [10.1093/mnras/stad2411](https://doi.org/10.1093/mnras/stad2411)
- . 2023b, arXiv e-prints, arXiv:2304.02026, doi: [10.48550/arXiv.2304.02026](https://doi.org/10.48550/arXiv.2304.02026)
- Oke, J. B., & Gunn, J. E. 1983, *ApJ*, 266, 713, doi: [10.1086/160817](https://doi.org/10.1086/160817)
- Osterbrock, D. E., & Ferland, G. J. 2006, *Astrophysics of gaseous nebulae and active galactic nuclei*
- Ouchi, M., Ono, Y., & Shibuya, T. 2020, *ARA&A*, 58, 617, doi: [10.1146/annurev-astro-032620-021859](https://doi.org/10.1146/annurev-astro-032620-021859)
- pandas development team, T. 2020, *pandas-dev/pandas: Pandas, latest*, Zenodo, doi: [10.5281/zenodo.3509134](https://doi.org/10.5281/zenodo.3509134)
- Papovich, C., Cole, J. W., Yang, G., et al. 2023, *ApJL*, 949, L18, doi: [10.3847/2041-8213/acc948](https://doi.org/10.3847/2041-8213/acc948)
- Pérez-González, P. G., Gil de Paz, A., Zamorano, J., et al. 2003, *MNRAS*, 338, 508, doi: [10.1046/j.1365-8711.2003.06077.x](https://doi.org/10.1046/j.1365-8711.2003.06077.x)
- Pérez-González, P. G., Rieke, G. H., Egami, E., et al. 2005, *ApJ*, 630, 82, doi: [10.1086/431894](https://doi.org/10.1086/431894)
- Pérez-González, P. G., Rieke, G. H., Villar, V., et al. 2008, *ApJ*, 675, 234, doi: [10.1086/523690](https://doi.org/10.1086/523690)
- Pérez-González, P. G., Barro, G., Rieke, G. H., et al. 2024a, arXiv e-prints, arXiv:2401.08782, doi: [10.48550/arXiv.2401.08782](https://doi.org/10.48550/arXiv.2401.08782)
- Pérez-González, P. G., Rinaldi, P., Caputi, K. I., et al. 2024b, arXiv e-prints, arXiv:2402.16942, doi: [10.48550/arXiv.2402.16942](https://doi.org/10.48550/arXiv.2402.16942)
- Perrin, M. D., Sivaramakrishnan, A., Lajoie, C.-P., et al. 2014, in *Society of Photo-Optical Instrumentation Engineers (SPIE) Conference Series*, Vol. 9143, *Space Telescopes and Instrumentation 2014: Optical, Infrared, and Millimeter Wave*, ed. J. Oschmann, Jacobus M., M. Clampin, G. G. Fazio, & H. A. MacEwen, 91433X, doi: [10.1117/12.2056689](https://doi.org/10.1117/12.2056689)
- Price, S. H., Suess, K. A., Williams, C. C., et al. 2023, arXiv e-prints, arXiv:2310.02500, doi: [10.48550/arXiv.2310.02500](https://doi.org/10.48550/arXiv.2310.02500)
- Prieto-Lyon, G., Strait, V., Mason, C. A., et al. 2023, *A&A*, 672, A186, doi: [10.1051/0004-6361/202245532](https://doi.org/10.1051/0004-6361/202245532)
- Ranalli, P., Comastri, A., Vignali, C., et al. 2013, *A&A*, 555, A42, doi: [10.1051/0004-6361/201321211](https://doi.org/10.1051/0004-6361/201321211)
- Rieke, G. H., Wright, G. S., Böker, T., et al. 2015, *PASP*, 127, 584, doi: [10.1086/682252](https://doi.org/10.1086/682252)
- Rieke, M., & the JADES Collaboration. 2023, arXiv e-prints, arXiv:2306.02466, doi: [10.48550/arXiv.2306.02466](https://doi.org/10.48550/arXiv.2306.02466)
- Rieke, M. J., Robertson, B., Tacchella, S., et al. 2023, *ApJS*, 269, 16, doi: [10.3847/1538-4365/acf44d](https://doi.org/10.3847/1538-4365/acf44d)
- Rigby, J., Perrin, M., McElwain, M., et al. 2023, *PASP*, 135, 048001, doi: [10.1088/1538-3873/acb293](https://doi.org/10.1088/1538-3873/acb293)
- Rinaldi, P., Caputi, K. I., Costantin, L., et al. 2023a, *ApJ*, 952, 143, doi: [10.3847/1538-4357/acdc27](https://doi.org/10.3847/1538-4357/acdc27)
- Rinaldi, P., Caputi, K. I., Iani, E., et al. 2023b, arXiv e-prints, arXiv:2309.15671, doi: [10.48550/arXiv.2309.15671](https://doi.org/10.48550/arXiv.2309.15671)
- Robertson, B. E., Tacchella, S., Johnson, B. D., et al. 2023, *Nature Astronomy*, 7, 611, doi: [10.1038/s41550-023-01921-1](https://doi.org/10.1038/s41550-023-01921-1)
- Rodighiero, G., Bisigello, L., Iani, E., et al. 2023, *MNRAS*, 518, L19, doi: [10.1093/mnras/slac115](https://doi.org/10.1093/mnras/slac115)
- Sanders, D. B., & Mirabel, I. F. 1996, *ARA&A*, 34, 749, doi: [10.1146/annurev.astro.34.1.749](https://doi.org/10.1146/annurev.astro.34.1.749)
- Schlafly, E. F., & Finkbeiner, D. P. 2011, *ApJ*, 737, 103, doi: [10.1088/0004-637X/737/2/103](https://doi.org/10.1088/0004-637X/737/2/103)
- Sérsic, J. L. 1963, *Boletín de la Asociación Argentina de Astronomía La Plata Argentina*, 6, 41
- Siebenmorgen, R., Heymann, F., & Efstathiou, A. 2015, *A&A*, 583, A120, doi: [10.1051/0004-6361/201526034](https://doi.org/10.1051/0004-6361/201526034)
- Sonnnett, S., Meech, K., Jedicke, R., et al. 2013, *PASP*, 125, 456, doi: [10.1086/670593](https://doi.org/10.1086/670593)
- Stalevski, M., Fritz, J., Baes, M., Nakos, T., & Popović, L. Č. 2012, *MNRAS*, 420, 2756, doi: [10.1111/j.1365-2966.2011.19775.x](https://doi.org/10.1111/j.1365-2966.2011.19775.x)
- Stalevski, M., Ricci, C., Ueda, Y., et al. 2016, *MNRAS*, 458, 2288, doi: [10.1093/mnras/stw444](https://doi.org/10.1093/mnras/stw444)
- Steidel, C. C., Giavalisco, M., Pettini, M., Dickinson, M., & Adelberger, K. L. 1996, *ApJL*, 462, L17, doi: [10.1086/310029](https://doi.org/10.1086/310029)
- Stone, C. J., Courteau, S., Cuillandre, J.-C., et al. 2023, *MNRAS*, doi: [10.1093/mnras/stad2477](https://doi.org/10.1093/mnras/stad2477)
- Sun, W., Ho, L. C., Zhuang, M.-Y., et al. 2024, *ApJ*, 960, 104, doi: [10.3847/1538-4357/acflf6](https://doi.org/10.3847/1538-4357/acflf6)
- Tacchella, S., McClymont, W., Scholtz, J., et al. 2024, arXiv e-prints, arXiv:2404.02194, doi: [10.48550/arXiv.2404.02194](https://doi.org/10.48550/arXiv.2404.02194)
- Taylor, M. 2011, *TOPCAT: Tool for OPERations on Catalogues And Tables*, *Astrophysics Source Code Library*, record ascl:1101.010. <http://ascl.net/1101.010>
- Tsai, C.-W., Eisenhardt, P. R. M., Wu, J., et al. 2015, *ApJ*, 805, 90, doi: [10.1088/0004-637X/805/2/90](https://doi.org/10.1088/0004-637X/805/2/90)
- Übler, H., Maiolino, R., Curtis-Lake, E., et al. 2023, *A&A*, 677, A145, doi: [10.1051/0004-6361/202346137](https://doi.org/10.1051/0004-6361/202346137)
- van Mierlo, S. E., Caputi, K. I., Ashby, M. L. N., et al. 2023, arXiv e-prints, arXiv:2311.17764, doi: [10.48550/arXiv.2311.17764](https://doi.org/10.48550/arXiv.2311.17764)
- Vanden Berk, D. E., Richards, G. T., Bauer, A., et al. 2001, *AJ*, 122, 549, doi: [10.1086/321167](https://doi.org/10.1086/321167)

- Virtanen, P., Gommers, R., Oliphant, T. E., et al. 2020, Nature Methods, 17, 261, doi: [10.1038/s41592-019-0686-2](https://doi.org/10.1038/s41592-019-0686-2)
- Wang, B., Fujimoto, S., Labbé, I., et al. 2023, ApJL, 957, L34, doi: [10.3847/2041-8213/acfe07](https://doi.org/10.3847/2041-8213/acfe07)
- Wang, B., de Graaff, A., Davies, R. L., et al. 2024, arXiv e-prints, arXiv:2403.02304, doi: [10.48550/arXiv.2403.02304](https://doi.org/10.48550/arXiv.2403.02304)
- Wang, T., Schreiber, C., Elbaz, D., et al. 2019, Nature, 572, 211, doi: [10.1038/s41586-019-1452-4](https://doi.org/10.1038/s41586-019-1452-4)
- Weaver, J. R., Zalesky, L., Kokorev, V., et al. 2023, ApJS, 269, 20, doi: [10.3847/1538-4365/acf850](https://doi.org/10.3847/1538-4365/acf850)
- Wes McKinney. 2010, in Proceedings of the 9th Python in Science Conference, ed. Stéfan van der Walt & Jarrod Millman, 56 – 61, doi: [10.25080/Majora-92bf1922-00a](https://doi.org/10.25080/Majora-92bf1922-00a)
- Whitaker, K. E., Labbé, I., van Dokkum, P. G., et al. 2011, ApJ, 735, 86, doi: [10.1088/0004-637X/735/2/86](https://doi.org/10.1088/0004-637X/735/2/86)
- Whitaker, K. E., Ashas, M., Illingworth, G., et al. 2019, ApJS, 244, 16, doi: [10.3847/1538-4365/ab3853](https://doi.org/10.3847/1538-4365/ab3853)
- Williams, C. C., Tacchella, S., Maseda, M. V., et al. 2023, ApJS, 268, 64, doi: [10.3847/1538-4365/acf130](https://doi.org/10.3847/1538-4365/acf130)
- Wright, G. S., Wright, D., Goodson, G. B., et al. 2015, PASP, 127, 595, doi: [10.1086/682253](https://doi.org/10.1086/682253)
- Wright, G. S., Rieke, G. H., Glasse, A., et al. 2023, PASP, 135, 048003, doi: [10.1088/1538-3873/acbe66](https://doi.org/10.1088/1538-3873/acbe66)
- Yan, H., Dickinson, M., Eisenhardt, P. R. M., et al. 2004, ApJ, 616, 63, doi: [10.1086/424898](https://doi.org/10.1086/424898)
- Yang, G., Caputi, K. I., Papovich, C., et al. 2023, ApJL, 950, L5, doi: [10.3847/2041-8213/acd639](https://doi.org/10.3847/2041-8213/acd639)